Palaeogeography, Palaeoclimatology, Palaeoecology 271 (2009) 329–342

Contents lists available at ScienceDirect

Palaeogeography, Palaeoclimatology, Palaeoecology

journal homepage: www.elsevier.com/locate/palaeo

Stratigraphy and palaeoenvironmental implications of Pleistocene and Holocene aeolian sediments in the Lhasa area, southern Tibet (China)

Knut Kaiser [a,*], Zhongping Lai [b], Birgit Schneider [c], Christoph Reudenbach [a], Georg Miehe [a], Helmut Brückner [a]

[a] Faculty of Geography, University of Marburg, 35032 Marburg, Germany
[b] Luminescence Dating Group, Key Laboratory of Salt Lake Resources and Chemistry, Chinese Academy of Sciences, 810008 Xining, China
[c] Department of Geography, University of Leipzig, 04103 Leipzig, Germany

ARTICLE INFO

Article history:
Received 7 December 2007
Received in revised form 31 October 2008
Accepted 3 November 2008

Keywords:
Loess
Aeolian sand
Luminescence and radiocarbon dating
Palaeosol
Human activity
Xizang–Qinghai Plateau

ABSTRACT

Along the middle and lower reaches of the Kyichu River and its tributaries (Lhasa area, southern Tibet), a multidisciplinary study was carried out in order to investigate the areal distribution, sedimentological properties, ages and palaeoenvironmental implications of aeolian deposits including intercalated palaeosols. This research was initiated to investigate to what extent southern Tibet is influenced by past human activity, as even recent evaluations perceive the present treeless desertic environment as natural. Fifteen profiles were recorded at an altitude of 3540–4580 m a.s.l. with subsequent sedimentological, geochronological (OSL, AMS ^{14}C) and palaeobotanical (charcoal) analyses. Sediment properties of both loesses and aeolian sands reveal an origin from aeolian sorting of nearby fluvial deposits. The calculated ages are the oldest obtained thus far on aeolian sediments from southern and interior Tibet, revealing natural aeolian sedimentation before and around the Last Glacial Maximum (c. 20 ka). However, a distinct portion of Late Holocene sandy aeolian sediments also occurs. Both the evidence for the aeolian dynamics (widespread Pleistocene loess and aeolian sand deposition, local Late Holocene aeolian sand deposition, modern reactivation of widespread Pleistocene aeolian sands) and the palaeobotanical findings (Late Holocene vegetation change from a tree-bearing to a widely treeless landscape) provide evidence that the Lhasa area was strongly influenced by human activity since at least the Late Neolithic (c. 4200 cal yrs BP). Thus the present-day desertic environment might not primarily be a result of the semiarid climate or the high-altitude conditions, but rather of activities of the humans and their collateral effects. However, once established, this semi-natural ecosystem persisted, controlled by strong grazing, firewood extraction, erosion and harsh edaphic conditions, preventing the recovery of trees.

1. Introduction

Aeolian dynamics are a characteristic of Central Asian landscapes and originate from the mainly arid climate conditions and specific atmospheric and geomorphic settings. During the cold stages of the Quaternary, the territory affected by aeolian processes was considerably enlarged due to the areal expansion of a cold and dry climate (Yang et al., 2004; Ding et al., 2005). However, human activity, mostly in the form of deforestation and agriculture, has intensified aeolian processes in vast areas with semiarid climate conditions in both the present and the recent past (Li et al., 2005; Huang et al., 2006; Sun et al., 2006). In China, for instance, desert expansion has accelerated with each successive decade since 1950. From 1994 to 1999 alone, the Gobi Desert expanded by 52,400 km^2 now reaching an area only 250 km north of Beijing (Brown, 2003). Thus, in general, tracing present day and predicting future aeolian dynamics is a vitally important environmental issue in Central Asia. However, both understanding the long-term scale (thousands of years) and identifying the causes (climate, geomorphic setting, humans) necessarily require past aeolian processes to be considered as an aspect of the landscape history.

The southern part of Central Asia is formed by the Tibetan Plateau, the largest alpine plateau in the world (c. 2.2×10^6 km^2). However, in comparison to the adjacent Chinese Loess Plateau, where research on both past and present-day geomorphic dynamics has been well-established for a long time (e.g. An et al., 1991; He et al., 2006), knowledge of the distribution pattern, sedimentological properties and dating of aeolian deposits on the Tibetan Plateau is still in an early stage.

Vast areas on the Plateau are covered by relatively thin aeolian mantles consisting of silty and sandy loesses and loess-like sediments (e.g. Clarke, 1995; Péwé et al., 1995; Lehmkuhl, 1997). The thickness of these deposits is often below 1 m, covering nearly all areas up to c.

* Corresponding author. Tel.: +49 64212824253; fax: +49 64212828950.
E-mail address: Knut.Kaiser@gmx.net (K. Kaiser).

0031-0182/$ – see front matter © 2008 Elsevier B.V. All rights reserved.
doi:10.1016/j.palaeo.2008.11.004

5000 m a.s.l. (Kaiser, 2007; Kaiser et al., 2008). However, at the northeastern margin of the Plateau and at altitudes proximately below the rim thick loess covers exist, which attain more than 20 m in the Aba Basin (c. 3500 m a.s.l.; Lehmkuhl, 1995) and c. 260 m around Xining (c. 2300 m a.s.l.; Kemp et al., 1996; Lu et al., 2004). Furthermore, coversands and sand dunes (= aeolian sands) of a few metres to decametres in thickness occur locally, mostly along the major rivers, in the foreland of glaciers and in intramontane basins (e.g. Liu and Zhao, 2001; Li et al., 2006; Porter and Zhou, 2006).

The few stratigraphical investigations on the Tibetan Plateau performed so far have been mainly focussed on dating aspects using luminescence ages of loesses and aeolian sands as well as radiocarbon ages of intercalated palaeosols. Most of the studies took place in northeast, east and central Tibet (e.g. Lehmkuhl et al., 2000; Fang et al., 2003; Stokes et al., 2003; Lu et al., 2004; Küster et al., 2006). Remarkably, despite the fact that only a few sequences with unquestionable dating control are available and comparably few sedimentological data exist, far-reaching models on the age of aeolian deposits and the sedimentary process have already been proposed (Lehmkuhl and Haselein, 2000; Porter and Zhou, 2006; Sun et al., 2007). Conversely, the possible role of humans in triggering Holocene aeolian processes has been considered only rudimentarily (Jäkel, 2002; Klinge and Lehmkuhl, 2003, 2005).

This paper presents results on the stratigraphy and sedimentology of aeolian deposits in southern Tibet. Our study area is the Kyichu ('Lhasa River') Valley and its tributaries, where the research project 'Holocene geomorphic genesis of the Kyichu catchment' was launched to clarify the more recent geomorphic and palaeoenvironmental history, continuing previous research on past human–environment relationships in that area (Miehe et al., 2003, 2006; Kaiser et al., 2006; Miehe et al., 2008a; Kaiser et al., in press; Fig. 1). As even recent evaluations perceive the present treeless desertic environment as natural, seemingly originating from the high altitude and / or semi arid climate conditions (Yu et al., 2001; Song et al., 2004; Luo et al., 2005), this research was initiated to access the extent that southern Tibet is influenced by past human activity. In the course of the project, and for the first time in southern and interior Tibet, Last Interglacial and Last Glacial aeolian sequences and corresponding palaeosols are detected, therefore the temporal focus comprises the last c. 100,000 years.

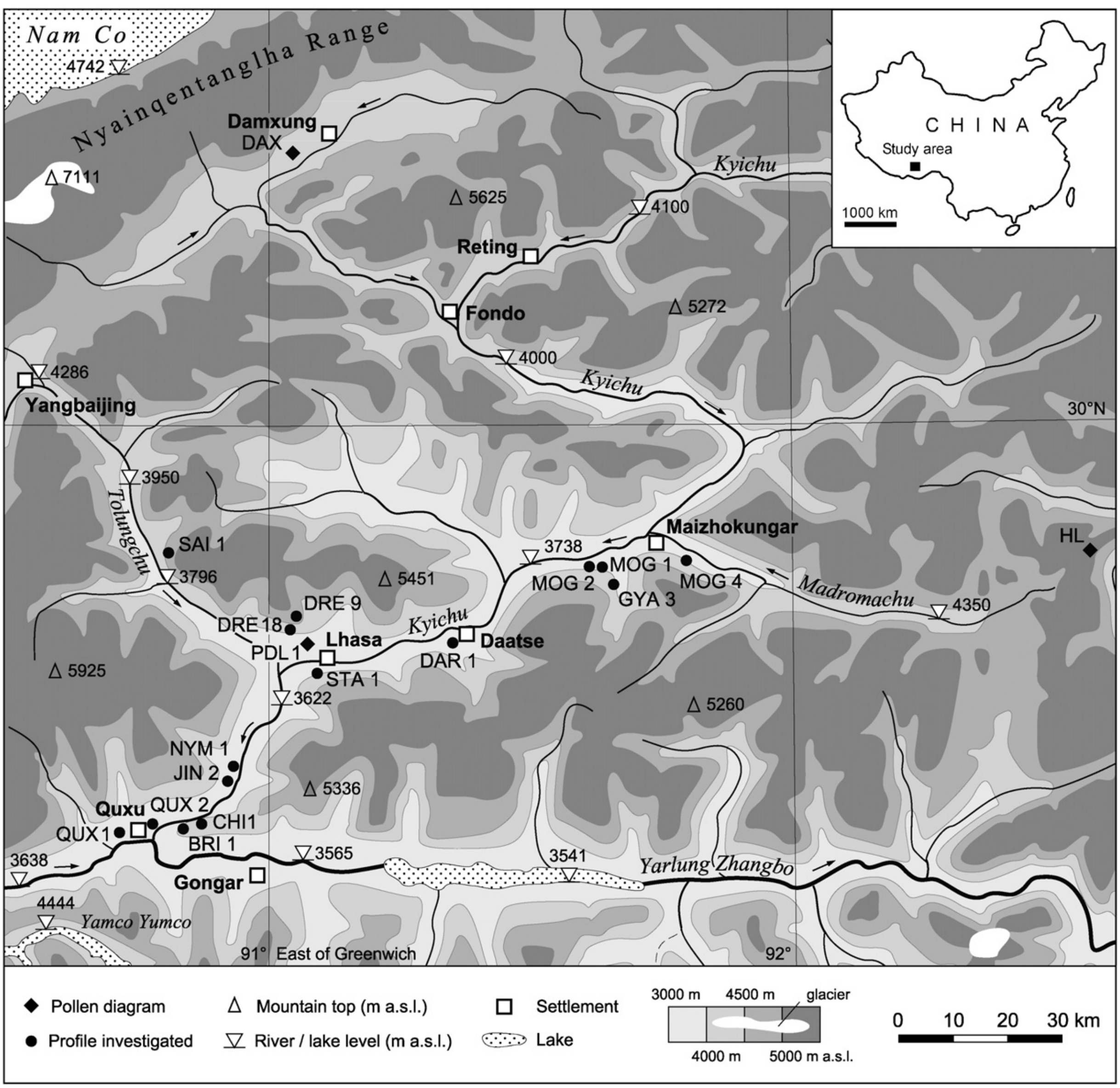

Fig. 1. Study area with the profiles recorded (map adapted from Atlas of Tibet Plateau, 1990). Abbreviations of pollen diagrams: PDL 1 = Lhasa 1, HL = 'Hidden Lake' / Co Qongjiamong, DAX = Damxung.

2. Setting

According to Lehmkuhl et al. (2002), southern Tibet is characterised vertically by the following geomorphic zones: (i) zone of fluvial processes and sand fields / dunes (up to c. 3800 m a.s.l.), (ii) zone of torrent valleys and gully erosion (up to c. 4200 m a.s.l.), (iii) zone of steppe gullies (up to c. 5100 m a.s.l.), and (iv) zone of periglacial processes (above c. 5100 m a.s.l.). The modern snowline is calculated at about 6000 m a.s.l.

The profiles recorded are located in the Kyichu Valley and its tributaries (Fig. 1). They belong to the catchment of the east-flowing Yarlung Zhangbo, which, after leaving the south-eastern Himalayas, flows west to India as the Brahmaputra. The changing flow directions of the Kyichu and its tributaries follow diversely trending tectonic structures (Atlas of Tibet Plateau, 1990). The lower river course from Maizhokungar to the mouth, in particular down valley from Lhasa, predominantly shows braiding with local anastomosing sections. The middle reach between Reting and Maizhokungar predominantly shows large-scale meandering with local anastomosing and braiding sections. The middle and lower valley sections have widths of 2–4 km comprising some larger basins, such as the Lhasa Basin (c. 3650 m a.s.l.), whose north–south dimension reaches c. 6 km. There are a lack of high-lying fluvial terraces in the middle and lower Kyichu Valley, which is explained by its aggradational character in a tectonically (sub-) active setting, permanently burying older valley bottoms by alluvial sedimentation (e.g. Lhasa Basin: c. 480 m of sedimentary infill; Kaiser et al., in press).

The predominant rock in the study area is granite accompanied by Carboniferous to Tertiary metamorphics and sediments, which are covered outside the valleys and basins by a thin veneer of Quaternary aeolian and colluvial sediments (Atlas of Tibet Plateau, 1990). Larger areas of active aeolian sands exist on the valley flanks in the river mouth area adjoining the Yarlung Zhangbo Valley (Fig. 2, Appendix A).

The present climate on the valley ground in Lhasa (c. 3650 m a.s.l.) is characterised by a mean annual air temperature of 7.7 °C, summer temperatures of more than 15.5 °C and winter temperatures below −2.1 °C (Domrös and Peng, 1988; Miehe et al., 2001). According to three meteorological stations available, the mean annual precipitation in the study area on the valley floors is 361 to 490 mm derived by c. 10-year (Gongar, Maizhokungar) to 40-year (Lhasa) series of measurements. There are six to seven months with relatively arid conditions (winter), suggesting a semiarid climate (Miehe et al., 2001). However, a distinct altitude-dependent climatic differentiation exists. Rainfall on the higher slopes is considerable higher as rain-gauge measurements in the Lhasa area show, with an annual rainfall of 485 mm at 3750 m a.s.l. (lower slope) and 715 mm at 4650 m a.s.l. (upper slope; Miehe et al., 2003). Domrös and Peng (1988) assign the Lhasa area to a semiarid subtype in the 'Temperate Plateau Zone' of the climate zones of China.

Human occupation of the Lhasa area is proven since the Late Neolithic (i.e. since c. 4200 cal yrs BP; Aldenderfer and Zhang, 2004; Kaiser et al., 2006). Livestock grazing and fuel-wood extraction is suggested to have widely replaced the natural vegetation, leaving behind partly eroded badlands (Miehe et al., 2003, 2006, 2008a). The floodplains are characterised by mobile cobbles to sands, sparsely overgrown by grasses and grazed wetlands with a dense cover of sedges, grasses and herbs, or, if inactive, by irrigated arable land and wood plantations. Only locally are grazed remains of the natural

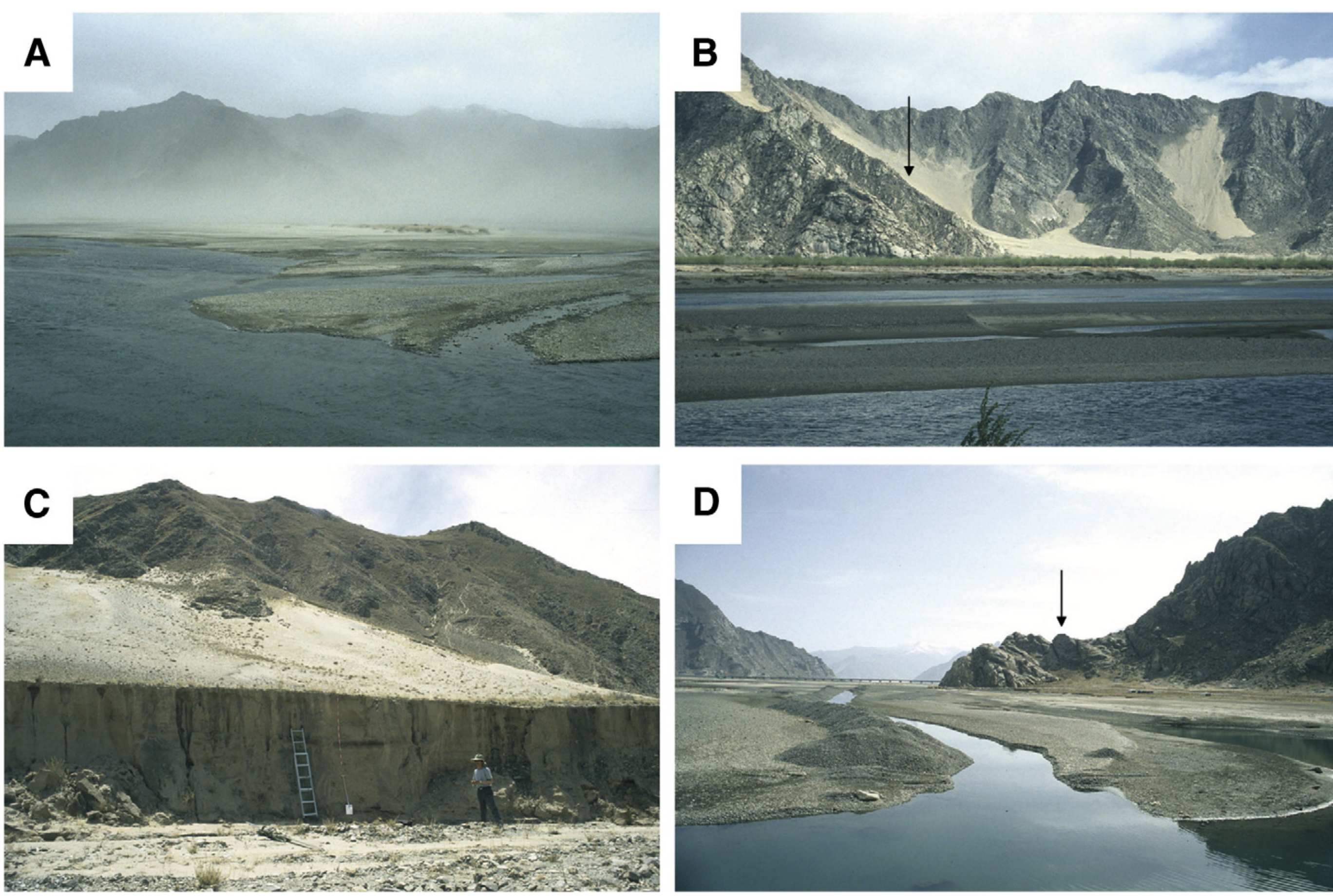

Fig. 2. Photos of selected sites investigated. (A) Drift-sand event on the floodplain of the Kyichu Valley (27 April 2006). (B) Active aeolian sand area on the southern valley flank of the Kyichu climbing up to c. 600 m above the floodplain. The arrow indicates the position of profile CHI 1 lying behind the rocky ridge. (C) Location of profile STA 1 showing an active aeolian sand area on the southern valley flank of the Kyichu. (D) Lower Kyichu Valley. The arrow indicates the position of profile BRI 1 lying below the rocky ridge.

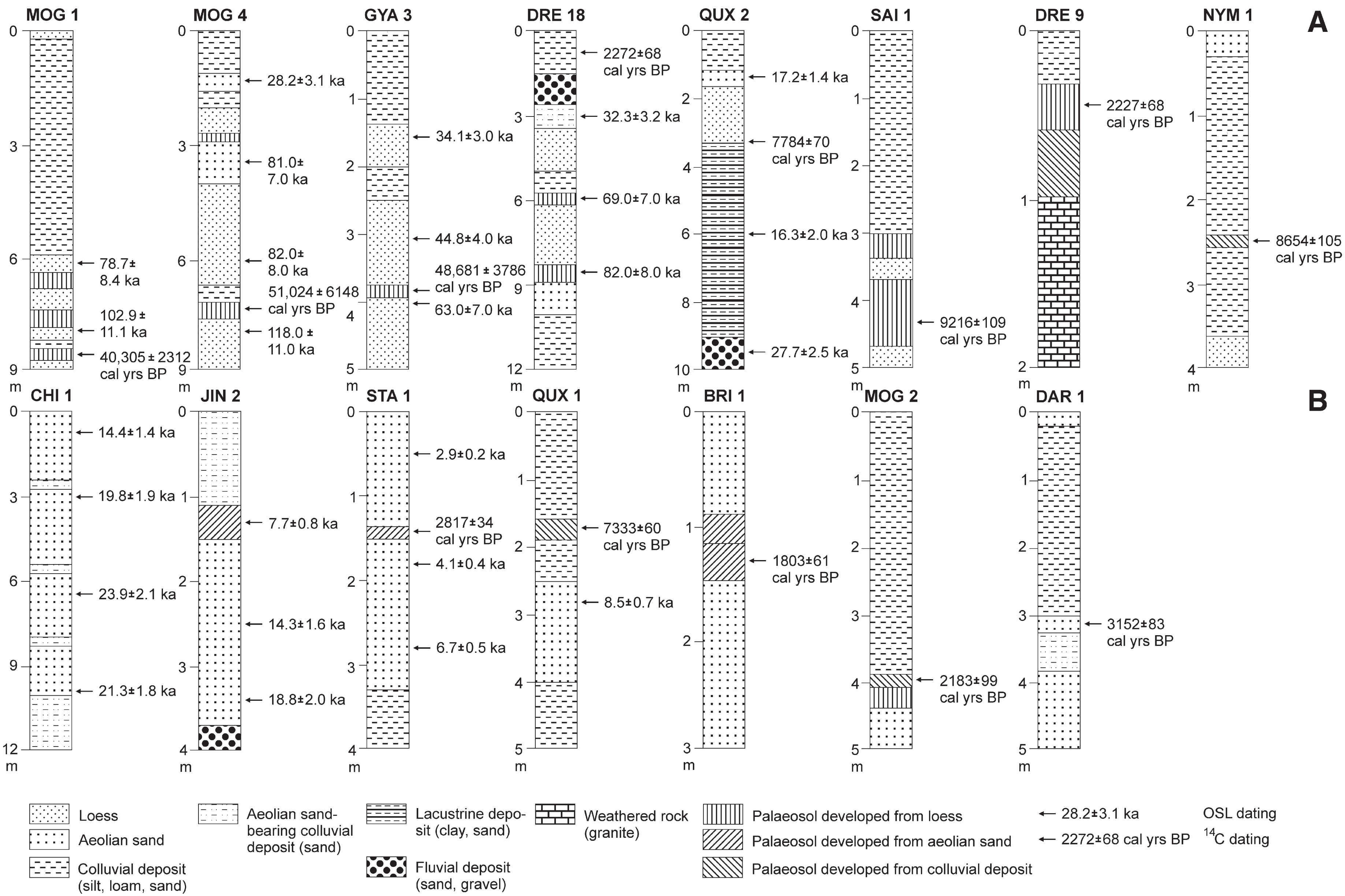

Fig. 3. Simplified logs of the profiles investigated alongside luminescence and radiometric dating results. (A) Profiles predominately having loess layers. (B) Profiles predominately having aeolian sand layers.

phreatophytic woodlands, consisting of buckthorn (*Hippophae* spp.), willow (*Salix* spp.) and poplar (*Populus* spp.), preserved. The valley slopes are exposed to a strong, year-round grazing influence, having a grass-dominated vegetation with low thorny shrubs (*Sophora moorcroftiana*) and wormwoods (*Artemisia* spp.). In some slope positions inaccessible for grazing, shrubs several metres high occur. Above c. 4500 m a.s.l. dense sedge mats of *Kobresia pygmaea* accompanied by cushions prevail. Dry-site forests or even single trees are very rare in the study area. The largest remnant of the former forest vegetation, proven by a comprehensive survey detecting several occurrences of small-scale juniper woodlands and trees in recent years (Miehe et al., 2008a), is a south-exposed mature juniper forest (*Juniperus tibetica*) around Reting Monastery, comprising trees of 10–15 m in height and up to c. 1000 years in age (c. 4200–4850 m a.s.l.; Miehe et al., 2003, 2007; Bräuning, 2007; Miehe et al., 2008a). Small remains of the natural forest vegetation on north-facing slopes consisting of birch (*Betula* spp.), willow (*Salix* spp.) and rhododendron (*Rhododendron* spp.) are preserved in the middle Kyichu Valley and the upper Madromachu Valley.

3. Materials and methods

3.1. Field record and sedimentology

In the study area, both loesses and aeolian sands were recorded. Loess can be defined simply as a terrestrial clastic sediment, composed predominantly of silt-size particles, formed essentially by the accumulation of wind-blown dust (Pye, 1995). Aeolian sands are characterised by a dominance of the sand-sized grain fraction, predominantly in the fine to medium sand class.

Field research for the 15 profiles presented here mainly took place in the spring of 2006. Both natural and anthropogenic exposures with thicknesses of 2–13 m were used after preparation of the sections (Figs. 1, 3 and 4). The profiles were described and sampled according to an international pedological standard (FAO, 2006). Designations of soil horizons and soil types are given using the 'World Reference Base for Soil Resources' (IUSS-ISRIC-FAO, 2006). The colours of sediments and soils were determined using the 'Munsell Soil Color Charts'. The content of coarse matter (>2 mm), comprising gravels to boulders,

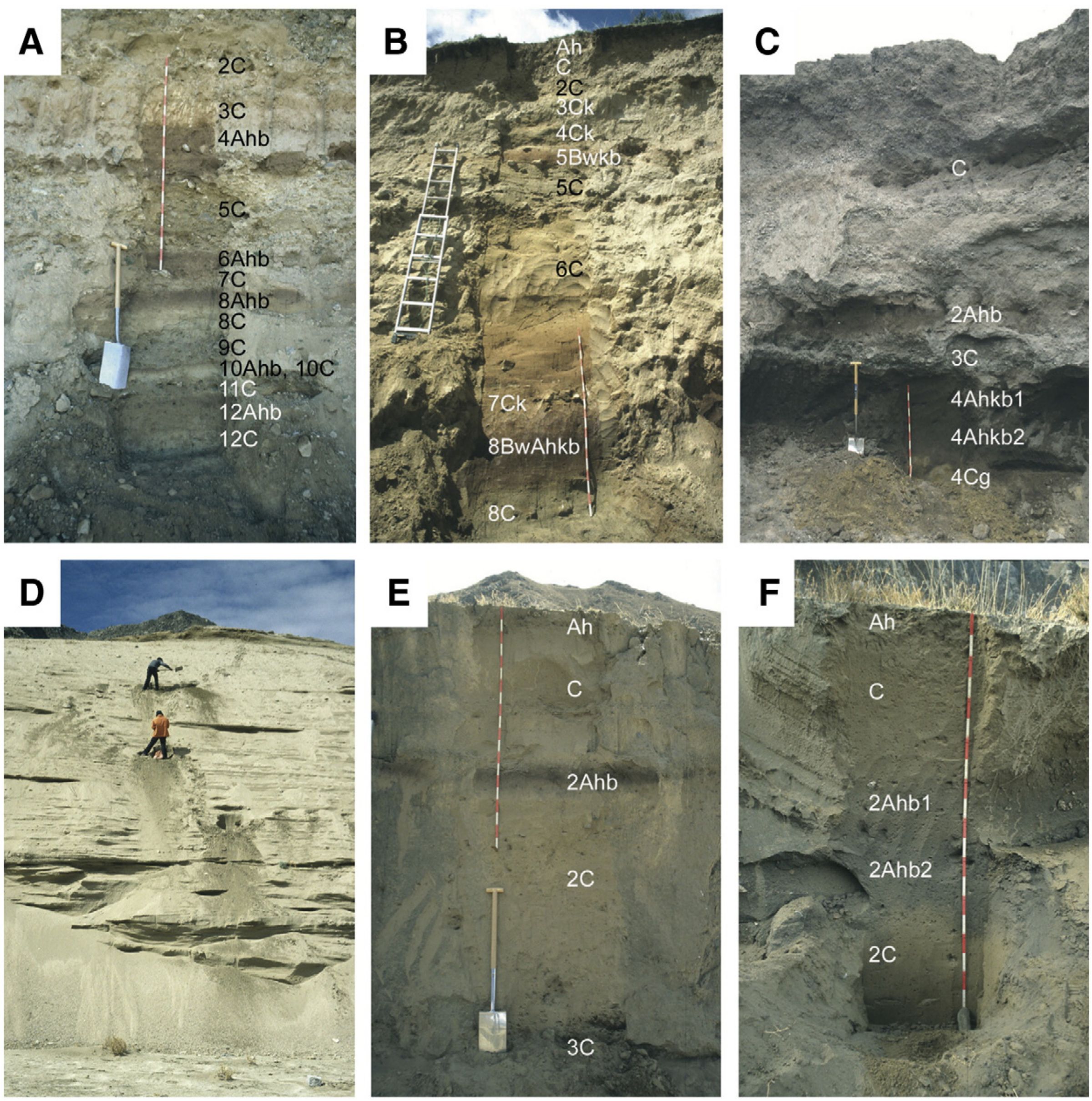

Fig. 4. Photos of selected profiles investigated. Soil horizons are also labelled. (A) Profile MOG 1 (length of the ruler = 200 cm). (B) Profile MOG 4 (length of the ruler = 200 cm). (C) Profile SAI 1 (length of the ruler = 110 cm). (D) Profile CHI 1. (E) Profile STA 1 (length of the ruler = 200 cm). (F) Profile BRI 1 (length of the ruler = 200 cm).

Table 1
Geographical site properties and sedimentological data of the profiles investigated from the Lhasa area

Sample	Altitude (m a.s.l.)	Northing	Easting	Sampling depth (cm)	Sediment classification	Soil horizon	Colour (Munsell)	Clay, silt, sand (%)	Textural class (FAO)	OC[a] (%)	$CaCO_3$ (%)	pH ($CaCl_2$)	EC[b] (mS cm^{-1})
MOG 4a	3894	29°47′30.0″	91°48′45.2″	0–40	Colluvial	Ah	10YR4/3	14, 48, 38	Loam	1.5	0.0	7.3	0.160
MOG 4b				200–270	Aeolian	4Ck	10YR5/6	22, 52, 26	Silt loam	0.3	10.2	8.0	0.110
MOG 4c				270–290	Aeolian	5Bwkb	7.5YR5/6	18, 52, 30	Silt loam	0.3	13.6	8.1	0.100
MOG 4d				290–390	Aeolian	5C	10YR5/4	6, 46, 48	Sandy loam	0.1	2.8	8.0	0.100
MOG 4e				410–670	Aeolian	6C	10YR5/6	11, 59, 30	Silt loam	0.2	1.5	8.0	0.080
MOG 4f				670–720	Colluvial	7Ck	10YR5/4	16, 62, 22	Silt loam	0.3	4.9	8.0	0.100
MOG 4g				720–760	Aeolian	8BwAhkb	7.5YR3/3	20, 52, 28	Silt loam	0.4	1.0	8.0	0.110
MOG 4h				760–900	Aeolian	8C	2.5YR6/3	5, 57, 38	Silt loam	0.1	0.0	8.0	0.060
MOG 1h	3778	29°47′57.0″	91°38′06.2″	0–20	Aeolian	Ah	10YR4/2	9, 50, 41	Silt loam	1.8	0.2	7.9	0.110
MOG 1a				600–640	Aeolian	3C	10YR6/6	12, 51, 37	Silt loam	0.1	0.2	7.8	0.100
MOG 1b				640–690	Aeolian	4Ahb	7.5YR4/3	13, 51, 36	Silt loam	0.4	0.1	7.8	0.070
MOG 1c				750–770	Aeolian	6Ahb	10YR4/3	12, 53, 35	Silt loam	0.3	0.2	7.8	0.090
MOG 1d				780–795	Aeolian	8Ahb	10YR4/3	17, 60, 23	Silt loam	0.3	0.0	7.7	0.070
MOG 1e				795–820	Aeolian	8C	10YR6/4	10, 52, 38	Silt loam	0.1	0.0	7.7	0.050
MOG 1f				860–885	Aeolian	12Ahb	10YR4/4	13, 52, 35	Silt loam	0.2	0.0	7.4	0.050
MOG 1g				885–900	Aeolian	12C	2.5Y5/3	7, 54, 39	Silt loam	0.1	0.0	5.7	0.060
GYA 3a	3840	29°44′54.6″	91°40′02.5″	250–380	Aeolian	4C	10YR5/6	15, 60, 25	Silt loam	0.2	1.3	8.0	0.090
GYA 3b				380–395	Aeolian	5Ahkb	10YR3/3	17, 68, 15	Silt loam	0.5	1.1	7.9	0.100
GYA 3c				395–450	Aeolian	5C	10YR5/4	11, 67, 22	Silt loam	0.2	1.3	8.0	0.070
DRE 18a	3707	29°40′09.7″	91°02′41.6″	0–20	Colluvial	Ah	10YR5/3	10, 40, 50	Loam	1.0	10.1	7.8	0.110
DRE 18b				260–350	Coll.-aeolian	4C	10YR7/3	5, 16, 79	Loamy sand	0.1	5.0	8.1	0.060
DRE 18c				350–500	Aeolian	5C	10YR7/3	20, 53, 27	Silt loam	0.3	15.5	8.0	0.180
DRE 18d				570–610	Aeolian	7B(k)wb	10YR4/4	19, 63, 18	Silt loam	0.2	3.9	8.0	0.110
DRE 18e				610–830	Aeolian	7C	2.5Y6/4	11, 66, 23	Silt loam	0.3	13.1	8.0	0.100
DRE 18f				830–880	Aeolian	8Bkwb	7.5YR5/4	14, 55, 31	Silt loam	0.4	16.8	7.9	0.110
DRE 18g				880–1000	Aeolian	8C	10YR5/4	12, 43, 45	Loam	0.2	5.1	8.0	0.100
QUX 2c	3536	29°21′57.3″	90°45′20.2″	110–160	Aeolian	2C	10YR6/2	3, 3, 94	Sand	0.1	0.0	7.9	0.050
QUX 2d				160–330	Aeolian	3C	10YR7/3	9, 63, 28	Silt loam	0.2	3.2	8.0	0.100
QUX 2e				330–650	Lacustrine	4C	10YR7/2	10, 34, 56	Sandy loam	0.4	0.0	8.0	0.080
QUX 2a				650–900	Lacustrine	5C	–	32, 58, 10	Silty clay loam	0.3	3.5	8.0	0.120
QUX 2b				900–1000	Fluvial	6C	–	4, 9, 87	Sand	0.1	0.6	8.0	0.050
CHI 1d	3618	29°21′47.9″	90°53′36.0″	0–20	Aeolian	Ah	10YR4/3	8, 47, 45	Loam	0.2	0.0	7.8	0.040
CHI 1c				50–70	Aeolian	C	2.5Y5/3	6, 45, 49	Sandy loam	0.1	0.0	7.6	0.020
CHI 1b				950–1000	Aeolian	C	2.5Y5/3	5, 27, 68	Sandy loam	0.2	0.0	8.1	0.060
CHI 1a				1040–1050	Aeolian	2C	2.5Y5/3	6, 10, 84	Loamy sand	0.2	0.0	8.0	0.060
JIN 2a	3597	29°25′38.7″	90°54′27.3″	110–150	Aeolian	2Bwb	10YR5/4	10, 34, 56	Sandy loam	0.2	0.0	7.8	0.040
JIN 2b				150–310	Aeolian	2C	10YR7/3	3, 2, 95	Sand	0.0	0.0	7.7	0.010
JIN 2c				310–370	Aeolian	3C	10YR5/3	6, 50, 44	Sandy loam	0.1	0.0	7.7	0.030
SAI 1a	3804	29°49′03.6″	90°45′25.0″	2–25	Colluvial	Ah	7.5YR4/2	15, 51, 34	Silt loam	1.4	12.7	7.9	0.950
SAI 1b				300–340	Aeolian	2Ahb	7.5YR4/2	19, 62, 19	Silt loam	1.0	10.6	7.9	0.110
SAI 1c				370–425	Aeolian	4Ahkb1	10YR3/3	19, 55, 26	Silt loam	1.0	6.7	8.0	0.120
SAI 1d				425–470	Aeolian	4Ahkb2	10YR3/3	21, 61, 18	Silt loam	1.0	6.1	7.9	0.140
SAI 1e				470–500	Aeolian	4Cg	10YR5/4	9, 55, 36	Silt loam	–	2.1	8.2	0.090
STA 1a	3658	29°37°59.4″	91°05′52.0″	0–15	Aeolian	Ah	10YR6/3	6, 17, 77	Loamy sand	0.5	0.0	7.4	0.030
STA 1b				15–135	Aeolian	C	10YR7/3	0, 14, 86	Loamy sand	0.1	0.0	7.4	0.050
STA 1c				135–150	Aeolian	2Ahb	10YR3/2	4, 20, 76	Loamy sand	0.7	0.0	7.4	0.020
STA 1d				150–330	Aeolian	2C	10YR7/3	5, 23, 72	Sandy loam	0.1	0.0	7.7	0.030
QUX 1a	3603	29°21′19.0″	90°43′25.1″	0–160	Colluvial	C	10YR6/3	7, 36, 57	Sandy loam	0.3	0.6	8.0	0.580
QUX 1b				160–190	Colluvial	2Ahb	10YR4/1	7, 38, 55	Sandy loam	1.7	1.0	7.8	0.160
QUX 1c				190–250	Colluvial	2C	10YR6/2	7, 31, 62	Sandy loam	0.3	1.2	7.9	0.160
BRI 1a	3566	29°21′58.1″	90°51′17.8″	15–90	Aeolian	C	10YR6/3	6, 24, 70	Sandy loam	0.2	0.0	7.8	0.060
BRI 1b				90–115	Aeolian	2Ahb1	10YR5/1	6, 23, 71	Sandy loam	0.7	0.0	7.9	0.050
BRI 1c				115–150	Aeolian	2C	10YR6/4	4, 16, 80	Loamy sand	0.1	0.0	7.8	0.030
NYM 1a	3600	29°26′55.1″	90°56′03.6″	0–30	Aeolian	Ah	10YR5/3	3, 44, 53	Sandy loam	0.4	0.0	7.6	0.060
NYM 1b				30–240	Colluvial	2C	10YR6/2	5, 29, 66	Sandy loam	0.3	0.0	7.7	0.210
NYM 1c				240–255	Colluvial	3Ah(k)b	10YR4/2	3, 45, 52	Sandy loam	0.8	0.2	7.9	0.280
NYM 1d				255–360	Colluvial	3C	10YR6/3	1, 29, 70	Sandy loam	0.2	0.0	7.8	0.160
NYM 1e				360–400	Aeolian	4C	2.5Y6/3	5, 56, 39	Silt loam	0.1	0.3	8.0	0.130
MOG 2a	3778	29°47′57.0″	91°38′06.2″	0–20	Colluvial	Ah	10YR5/3	11, 57, 32	Silt loam	2.5	0.0	5.0	0.060
MOG 2b				200–230	Colluvial	2C1	10YR5/4	8, 43, 49	Loam	0.2	0.0	7.6	0.050
MOG 2c				260–260	Colluvial	2C2	10YR4/3	12, 49, 39	Loam	0.3	0.0	7.5	0.040
MOG 2d				260–390	Colluvial	2C3	10YR5/4	10, 50, 40	Loam	0.2	0.0	7.6	0.050
MOG 2e				390–410	Coll.-aeolian	3Ahgb1	10YR3/2	15, 55, 30	Silt loam	0.6	0.0	7.5	0.050
MOG 2f				410–440	Aeolian	4Ahgb2	10YR4/2	15, 55, 30	Silt loam	0.5	0.0	7.5	0.050
MOG 2g				440–500	Aeolian	4Cg	10YR4/3	9, 44, 47	Loam	0.2	0.0	7.4	0.030
DRE 9a	4583	29°41′42.1″	91°03′01.8″	10–20	Colluvial	BwC	10YR5/4	13, 29, 58	Loam	–	0.0	6.6	0.052
DRE 9b				30–57	Aeolian	2AhBwb	10YR4/2	15, 50, 35	Silt loam	–	0.0	6.6	0.020
DRE 9c				72–97	Colluvial	3Bwb	10YR5/6	5, 19, 76	Loamy sand	–	0.0	6.6	0.018

[a] OC = organic carbon.
[b] EC = electrical conductivity.

was estimated in the field. All of the following analyses were performed on the matrix matter <2 mm (Table 1, Appendix A).

After air drying, careful hand-crushing, humus and carbonate destruction (H_2O_2 30%, HCL 10%) and dispersion with sodium pyrophosphate, a combined pipette and sieving test was used to determine the grain-size distribution. The grain-size terms used, 'fine, medium and coarse (-grained) sand', are defined by the mesh-sizes <0.2 mm, <0.63 mm and <2.0 mm respectively (FAO, 2006). Organic carbon (OC) was measured by dry combustion (Elementar vario EL) at 1100 °C in duplicates. $CaCO_3$ was determined volumetrically. Soil pH was analysed potentiometrically in 0.01 M $CaCl_2$ (soil: solution ratio = 1: 2.5). Electrical conductivity (EC) was measured by means of an electrode in distilled water (soil: solution ratio = 1: 2.5).

3.2. Geochronology

3.2.1. Radiocarbon dating

Thirteen samples of different material (charcoal, bulk-soil matter, bone) were extracted from the profiles and subsequently analysed in the Erlangen AMS Radiocarbon Laboratory, Germany (Table 2). The charcoal dated originated from palaeosols and various sediments. It was extracted macroscopically from the profiles and botanically determined in the Langnau Laboratory of Quaternary Woods (W.H. Schoch). Bulk-soil samples were pre-treated by the removal of roots and the acid–alkali–acid (AAA) method in order to remove carbonates and mobile humic substances, which otherwise might affect the ^{14}C results (Scharf et al., 2007). The soil organic matter fraction dated consists of *humins*, which are considered to be a reliable material for ^{14}C dating in soils (Pessenda et al., 2001). Any comparisons of ^{14}C dates with luminescence ages have to be based on the calibrated radiocarbon ages (cal yrs BP-values). The calibration of the ^{14}C dates was performed using the program 'CalPal-2007' (Weninger et al., 2007).

3.2.2. Luminescence dating

Due to anomalous fading, luminescence ages using feldspars would be underestimated (Lai and Brückner, 2008). Thus, in this study, optically stimulated luminescence (OSL; stimulation blue light LEDs, $\lambda = 470 \pm 20$ nm) of the quartz grain size 38–63 µm was carried out at the Marburg Luminescence Laboratory using a Risø TL-DA 15 reader. It has been shown that OSL dating using quartz grain size of 38–63 µm is suitable for aeolian sediments, with the convenience of avoiding the dangerous HF acid (Lai and Wintle, 2006; Lai et al., 2007). The purity of quartz extraction was checked using IR stimulation before equivalent dose determination. OSL signals were measured at 130 °C, and recorded for 60 s through two U-340 glass filters. The radioisotope concentrations were measured by inductively coupled plasma mass spectrometry (ICP-MS) at Cologne University, Germany. A water content of 10 ± 5% was assumed for age calculation, although the natural water content of the samples was generally lower (Kaiser et al., 2006). The sampled sections were opened some months to some years ago and hence they do not contain the original moisture. The cosmic-ray dose rate was estimated according to Prescott and Hutton (1994). Single aliquot regenerative-dose (SAR) protocol (Murray and Wintle, 2000) was used for equivalent dose determination. A laboratory dose recovery test was performed on samples GYA 3B (loess) and CHI 1C (aeolian sand), with preheat temperature varying from 220 to 300 °C (preheat time: 10 s; cut-heat: 220 °C for 10 s; test dose: 11 Gy; OSL was recorded at 130 °C for 60 s; four aliquots for each temperature point, and 20 aliquots in total). The applied laboratory doses are 50 and 95 Gy for sample GYA 3B and CHI 1C, respectively. For sample GYA 3B, a preheat plateau was observed for all temperatures applied. The average recovered equivalent dose for the 20 aliquots is 50.9 ± 0.5 Gy, and the average recovered equivalent dose for the 4 aliquots for each temperature point ranges from 49.1 ± 0.9 to 52.7 ± 1.5 Gy. For sample CHI 1C, a preheat plateau was observed for temperatures from 220 to 280 °C. The average recovered equivalent dose for the 16 aliquots falling into the plateau is 90 ± 2 Gy. As a result, the ratios of the measured to the known doses are 1.02 (GYA 3B) and 0.95 (CHI 1C). The results suggest that the recovered equivalent dose is insensitive to the preheat temperatures used, and that a known laboratory dose can be successfully recovered using the SAR protocol. Consequently, the preheat temperature was chosen to be 260 °C for 10 s. The decay curves show that the OSL signal is dominated by the fast component and that the recuperation is insignificant (Appendix A). The growth curves (Appendix A) were fitted using a single saturation exponential plus linear function. For equivalent dose calculation, the OSL of the first 0.96 s of stimulation was used (background extracted; Table 3). For most of the aliquots of the samples, the recycling ratio falls into the range of 0.9–1.1. All aliquots outside this range were rejected. The final equivalent dose (ED) for a sample was the average of ED for all aliquots, and the standard error of the mean ED was estimated from the ED distribution of a set of aliquots. As the quartz grains were not HF etched, the alpha efficiency was taken as 0.035 ± 0.003 (Lai et al., 2008). The final OSL age and the associated standard error for each sample are listed in Table 3.

4. Results

4.1. Areal distribution pattern

Nearly the whole study area is covered by a mostly thin veneer (<1 m) of aeolian sediments except active fluvial and peat bog sites, screes or barren rocks. On slopes, generally an areal pattern consisting of (vegetated) aeolian and colluvial layers, accumulations of boulders, screes and patches of barren rock occur. Only locally, particularly on footslope positions, does the thickness of loesses and aeolian sands

Table 2
Radiocarbon data of the profiles investigated from the Lhasa area. ^{14}C ages are given with 1-sigma probability. Calibration of the ^{14}C ages was performed using the program 'CalPal-2007' (Weninger et al., 2007)

Profile	Depth (cm)	Material dated	Lab. no.	$\delta^{13}C$ (‰)	^{14}C age (yrs BP)	^{14}C cal age (cal yrs BP)
MOG 4	720–760	Charcoal (mixed spectrum)	Erl-10120	−22.6	45,682 ± 5438	51,024 ± 6148
MOG 1	860–885	*Lonicera* sp. charcoal	Erl-10123	−25.5	36,273 ± 2327	40,305 ± 2312
GYA 3	380–395	Rosaceae / Maloideae charcoal	Erl-10119	−24.4	44,235 ± 3388	48,681 ± 3786
DRE 18	60–80	Bone	Erl-10125	−17.4	2285 ± 40	2272 ± 68
QUX 2	325–330	Deciduous wood charcoal	Erl-10946	−24.8	6943 ± 65	7784 ± 70
SAI 1	425–440	Bulk-soil matter	Erl-10122	−19.8	8233 ± 68	9216 ± 109
STA 1	135–150	*Juniperus* sp. charcoal	Erl-10940	−20.9	2713 ± 38	2817 ± 34
QUX 1	160–190	Bulk-soil matter	Erl-10124	−23.0	6381 ± 55	7333 ± 60
BRI 1	115–150	*Sophora* sp. charcoal	Erl-10938	−24.8	1865 ± 51	1803 ± 61
NYM 1	240–255	*Sophora* sp. charcoal	Erl-10939	−24.8	7827 ± 70	8654 ± 105
MOG 2	390–410	*Betula* sp. charcoal	Erl-10942	−25.5	2159 ± 51	2183 ± 99
DAR 1	300–325	*Hippophae* sp. charcoal	Erl-10948	−25.5	2970 ± 52	3152 ± 83
DRE 9	30–57	*Juniperus* sp. charcoal	Erl-6777	−21.0	2194 ± 41	2227 ± 68

Table 3
Optical dating (OSL) results and radioisotope concentrations of the profiles investigated from the Lhasa area

Lab. no.	Sample	Depth (cm)	U (ppm)	Th (ppm)	K (%)	Th: U (ratio)	Dose rate (Gy ka^{-1})	Water cont. (%)	ED[a] (Gy)	OSL age (ka)
MR0545	STA 1A	50	2.76±0.19	17.33±1.21	2.72±0.14	6.28	4.76±0.36	10±5	14±0.4	2.9±0.2
MR0546	STA 1B	180	2.69±0.18	17.34±1.21	2.68±1.13	6.45	4.64±0.36	10±5	19±1.1	4.1±0.4
MR0547	STA 1C	280	3.10±0.22	18.73±1.31	2.65±0.13	6.04	4.78±0.37	10±5	32±0.6	6.7±0.5
MR0548	CHI 1F	70	2.66±0.19	18.4±1.29	2.79±0.14	6.77	4.86±0.37	10±5	70±4	14.4±1.4
MR0549	CHI 1E	300	2.83±0.20	18.3±1.28	2.86±0.14	6.47	4.86±0.38	10±5	96±5	19.8±1.9
MR0550	CHI 1C	650	2.33±0.16	15.28±1.07	2.45±0.12	6.56	4.05±0.32	10±5	97±4	23.9±2.1
MR0551	CHI 1B	1000	2.86±0.20	17.21±1.21	2.95±1.15	6.02	4.74±0.38	10±5	101±3	21.3±1.8
MR0552	QUX 2A	130	1.92±0.13	11.36±0.79	2.63±0.13	5.92	4.01±0.31	10±5	69±2	17.2±1.4
MR0553	QUX 2B	600	2.71±0.19	17.71±1.24	2.67±0.13	6.54	4.48±0.34	10±5	73±7	16.3±2.0
MR0554	QUX 2C	950	2.74±0.19	15.5±1.08	2.45±0.12	5.66	4.09±0.31	10±5	113±5	27.7±2.5
MR0555	MOG 4A	130	3.45±0.24	22.26±1.56	2.33±0.12	6.45	4.93±0.37	10±5	139±11	28.2±3.1
MR0556	MOG 4C	350	2.99±0.21	18.21±1.28	2.29±0.12	6.09	4.39±0.34	10±5	354±12	81.0±7.0
MR0557	MOG 4E	600	3.25±0.23	20.62±1.44	2.48±0.12	6.34	4.73±0.37	10±5	388±19	82.0±8.0
MR0558	MOG 4F	800	3.15±0.22	16.76±1.17	2.37±0.12	5.32	4.29±0.33	10±5	506±29	118.0±11.0
MR0559	GYA 3A	160	3.0±0.21	19.46±1.36	2.31±0.12	6.48	4.52±0.34	10±5	154±7	34.1±3.0
MR0560	GYA 3B	320	3.04±0.21	18.58±1.30	2.34±0.12	6.11	4.50±0.34	10±5	202±9	44.8±4.0
MR0561	GYA 3C	400	1.92±0.13	11.36±0.80	2.63±0.13	5.92	4.45±0.34	10±5	279±24	63.0±7.0
MR0562	DRE 18A	330	3.26±0.23	21.00±1.47	2.44±0.12	6.44	4.79±0.37	10±5	155±10	32.3±3.2
MR0563	DRE 18B	590	5.46±0.38	19.55±1.37	1.91±0.09	3.58	4.72±0.36	10±5	326±23	69.0±7.0
MR0564	DRE 18C	850	3.59±0.25	21.99±1.54	2.18±0.11	6.12	4.61±0.36	10±5	377±19	82.0±8.0
MR0565	QUX 1A	280	2.15±0.11	15.20±1.06	2.82±0.19	7.07	4.00±0.30	10±5	34±1	8.5±0.7
MR0566	JIN 2A	130	2.68±0.13	13.91±0.97	2.19±0.15	5.19	4.28±0.33	10±5	33±2	7.7±0.8
MR0567	JIN 2B	250	2.76±0.14	13.08±0.92	2.04±0.14	7.76	4.20±0.33	10±5	60±5	14.3±1.6
MR0568	JIN 2C	340	2.63±0.13	20.4±1.43	3.24±0.23	7.01	4.90±0.38	10±5	92±7	18.8±2.0
MR0569	MOG 1A	600	2.09±0.10	14.66±1.03	2.36±0.16	7.01	3.67±0.29	10±5	289±21	78.7±8.4
MR0570	MOG 1B	800	2.04±0.10	17.08±1.19	2.90±0.20	8.37	3.98±0.31	10±5	410±31	102.9±11.1

[a] equivalent dose.

exceed 5 m. The maximal thicknesses of loess-bearing and aeolian sand sequences exceed 9 m (MOG 4) and 12 m (CHI 1) respectively. The spatially predominant aeolian sediment is loess. The highest occurrence of a loess layer investigated is 4583 m a.s.l. (DRE 9). However, according to our own observations, thin loess layers can be found in the Lhasa area at least up to c. 5000 m a.s.l. (Kaiser et al., 2006; Kaiser, 2007).

Down valley from Maizhokungar, and paralleled by wide and temporarily dry floodplain sections, larger areas with aeolian sands occur on the valley slopes. These are mostly stabilised by vegetation. Up valley from Maizhokungar, the fairly narrow valley seemingly has a few occurrences of stabilised aeolian sands alone. In the lowermost section of the Kyichu Valley, active aeolian sands cover larger areas (Fig. 2). The largest active sand occurrence observed attained edge lengths of 1.5 km to 3.0 km (Appendix A). In general, the sands cover the distal parts of the (former) Kyichu floodplain and climb up the valley flanks. In places, they reach crest positions at about 4200 m a.s.l. and more. Thus the vertical extension of aeolian sand areas can amount to more than c. 600 m, partly joining the Yarlung Zhangbo catchment by traversing the watershed. Between the Kyichu and the *active* aeolian sand areas, there is a strip of irrigated arable land and woodlands forming a barrier of *potential* aeolian sand transport from the river to the slopes (Appendix A).

4.2. Sedimentological properties

There are a total of eight profiles having predominately loess layers and of seven profiles having predominately aeolian sand layers (Figs. 3 and 4). Most profiles were recorded at footslope and lower slope positions (n=11). Furthermore, an alluvial fan (DRE 18), a fluvial-lacustrine terrace (QUX 2), a weakly inclined aeolian sand area (CHI 1) and a middle-slope position (DRE 9) were investigated. In general, the profile composition is highly variable, comprising several small-scale changes of sediment types. All data and information presented refer to Table 1.

The loess layers investigated mostly have a massive structure without visible layering. Depending on the mineral content, the presence or absence of $CaCO_3$ and further factors (e.g. weak pedogenic imprint, groundwater influence), the loess colours mostly are brownish and yellowish. Partly, a small portion (usually below 1% by weight) of dispersedly distributed coarse particles occurs mostly in cobble size, which derive from rock fall due to the alpine relief of the study area. In most cases steep slopes with 20–40° inclination or vertical rock cliffs of hundreds of metres height occur above the loess-bearing profiles recorded. This geomorphological setting has caused the occasional synsedimentary input of coarse particles in predominantly wind-blown sediments. The 28 loess samples analysed represent, without exception, the 'silt loam' textural class (Fig. 5A), which consists of a dominant portion of silt and secondary portions of sand and clay. The silt fraction is predominantly coarse silt (Appendix A). The $CaCO_3$ content strongly varies. Five profiles have no or only a very small $CaCO_3$ content, whereas four profiles have higher contents (up to 16.8%). Mostly, if occurring, the highest $CaCO_3$ contents per profile will be reached in a palaeosol horizon, where the carbonate is secondarily enriched. Larger carbonate nodules are rare; loess-snails were never observed. The OC content is predominantly below the detectable limit. Both values of pH and EC indicate non-saline site conditions (Table 1).

The aeolian sand layers investigated have in cases of a great thickness (CHI 1, JIN 2, STA 1, BRI 1) a well-developed layering mostly in the form of parallel bedding (Fig. 4D). Their colours consist of brownish hues. The aeolian sands have no coarse matter >2 mm except profile CHI 1, where some interstratified thin layers of colluvial origin (slope wash) yielded a certain amount of gravels to pebbles (20–30%). Mostly, the aeolian sands occur in levelled parts of the landscape, such as floodplain sections and footslopes. This explains why there were no coarse components, in contrast to the loess. The 19 aeolian sand samples analysed represent a wide range of textural classes comprising sands and loams (Fig. 5A). The dominant sand fraction amounts to 44–95%. In general, sand-dominated grain-size fractions can be further subdivided according to the proportions of fine, medium and coarse sands in the sand fraction. These proportions are calculated apart from the total grain-size distribution, taking the proportions of different sand classes as a percentage of the total sand

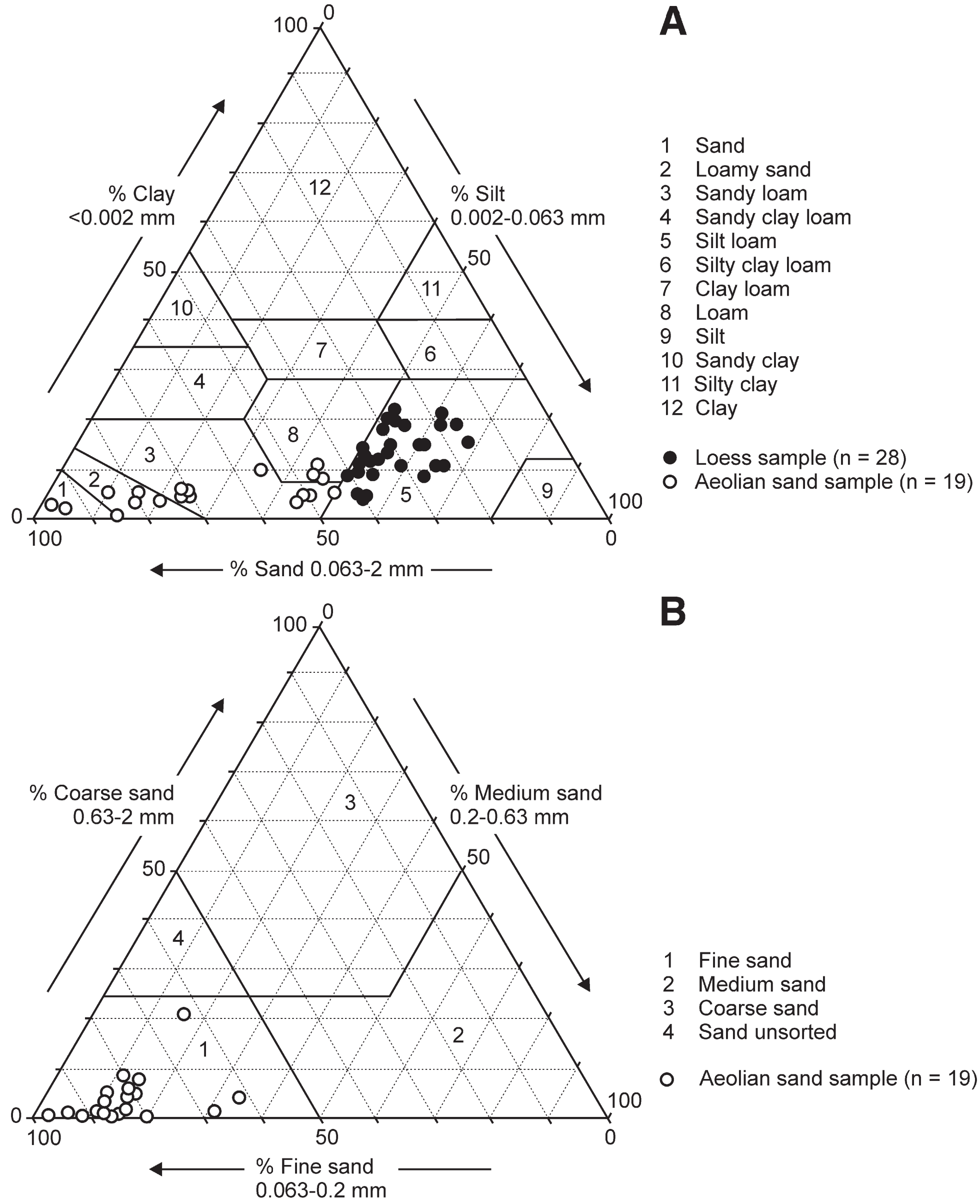

Fig. 5. Ternary diagrams showing textural classes of the aeolian sediment samples analysed (classification after FAO, 2006). (A) Loess and aeolian sand samples comprising the proportions of clay, silt and sand. (B) Aeolian sand samples comprising the sand grain-size sub-classes only.

content. Accordingly, all aeolian sand samples cluster in the fine sand class (Fig. 5B). The aeolian sands are carbonate-free except two profiles (MOG 4, DRE 18), where the $CaCO_3$ content amounts to 2.8–5.1%. The OC content is predominantly below the limit of detection. The pH and EC data indicate non-saline site conditions (Table 1).

Corresponding to the alpine relief, more or less thick colluvial deposits exist in the profiles, reaching a maximal thickness of c. 6 m in profile MOG 1 (Fig. 3). They mainly consist of loams, silty loams and sandy loams, having a distinct portion of coarse matter (gravels to boulders; up to 70%). Unlike the loess, the colluvial strata are well-layered, occasionally showing small-scale changes of colluvial and loess-aeolian events. As the colluvial matter partly comes from the relocation of loesses, it has a similar grain-size distribution of the fine component. Regarding their sub-facies, the colluvial deposits detected can be divided into (i) packages of alternating coarse-grained colluvial and fine-grained loess-aeolian sediments (e.g. MOG 1), (ii) coarse-grained sediments with a high proportion of cobbles and boulders originating from alluvial fans (e.g. DRE 18), (iii) matrix-supported sediments with only some cobbles and boulders originating from combined colluvial processes of hillwash plus rock fall (e.g. MOG 4), (iv) periglacial solifluction deposits (e.g. GYA 3), and (v) more or less fine-grained sediments originating from hillwash (e.g. DRE 9). Depending on the origin of the colluvial matter and the position in the stratigraphy, forming the sub- or the topsoil, both OC content and $CaCO_3$ content strongly vary. Even the colours are highly variable (Table 1). A specific sediment type consists of a mixture of aeolian sand and colluvial gravel and pebbles (certain layers in DRE 18, CHI 1, JIN 2).

Buried palaeosols (Nettleton et al., 2000; Krasilnikov and Garcia Calderon, 2006) occur in twelve of the fifteen profiles presented. Five profiles have two or more palaeosols (Fig. 3). According to the lack of properties indicating redistribution (e.g. layering, soil clasts, enrichment of coarse particles), the palaeosols can be regarded as formed *in-situ*. In total, 20 palaeosols were detected, predominantly developed on loesses. Further parent materials are aeolian sands and colluvial deposits. Several palaeosol types have been detected (Kastanozems, Phaeozems, Chernozems, Calcaric Cambisols, Cambisols, Arenosols, Regosols, Gleysols; IUSS-ISRIC-FAO, 2006). Most of the palaeosols developed from loesses are Kastanozems, whereas most of the palaeosols developed from aeolian sands are Arenosols. The palaeosol thickness varies between 15 and 100 cm with a mean thickness of 35 cm. The dominant colour is brown; sometimes with a greyish or yellowish colouring. Corresponding to the different site conditions, OC and $CaCO_3$ contents as well as pH values strongly vary. The EC data indicate non-saline site conditions (Table 1).

Most of the palaeosols bear macroscopic charcoal, allowing extraction for botanical determination and ^{14}C dating. The charcoal dated comprises both tree species (*Betula*, *Hippophae*, *Juniperus*) and shrub species (*Lonicera* = honeysuckle, Rosaceae / Maloideae = pip / stone fruit family, *Sophora* = pagoda tree) as well as deciduous wood of uncertain genus (Table 2).

4.3. Dating

In general, luminescence (OSL) datings of aeolian deposits commonly yield *sedimentation ages*, whereas radiocarbon age determination of intercalated palaeosols, depending on their stratigraphic position, either *predate or postdate* aeolian sedimentation (and sometimes both).

Nine of the 15 profiles investigated have OSL age control (total number = 26), partly in combination with controlling ^{14}C ages (Fig. 3, Tables 2 and 3). A broad range of sediments were dated (loess, aeolian sand, mixed aeolian sand-colluvial deposit, lacustrine clay, fluvial sand). Multi-level dating is available for most of the profiles, providing a check for the stratigraphical order and thus for reliability. The normal distribution of equivalent doses within a sample (>12 aliquots) determined by the SAR protocol shows that the samples were well bleached before deposition (Appendix A). The conditions adopted for the SAR protocol were verified by the successful laboratory dose recovery test. Thus the OSL dates presented can be regarded as reliable.

However, the five OSL ages >79 ka in profiles MOG 1, MOG 4 and DRE 18 should be regarded as minimum ages due to the fact that equivalent doses are approaching the saturation level in the growth curve of quartz OSL. However, as the dates are in stratigraphic order they do provide reliable relative chronological information.

A total of 24 OSL datings on loess (n = 9) and aeolian sand (n = 15) were determined. The loess ages have a range of 118.0 ± 11.0 to 34.1 ± 3.0 ka, whereas the aeolian sand ages range from 81.0 ± 7.0 to 2.9 ± 0.2 ka (Fig. 6A). In terms of chronozones, loesses are exclusively older

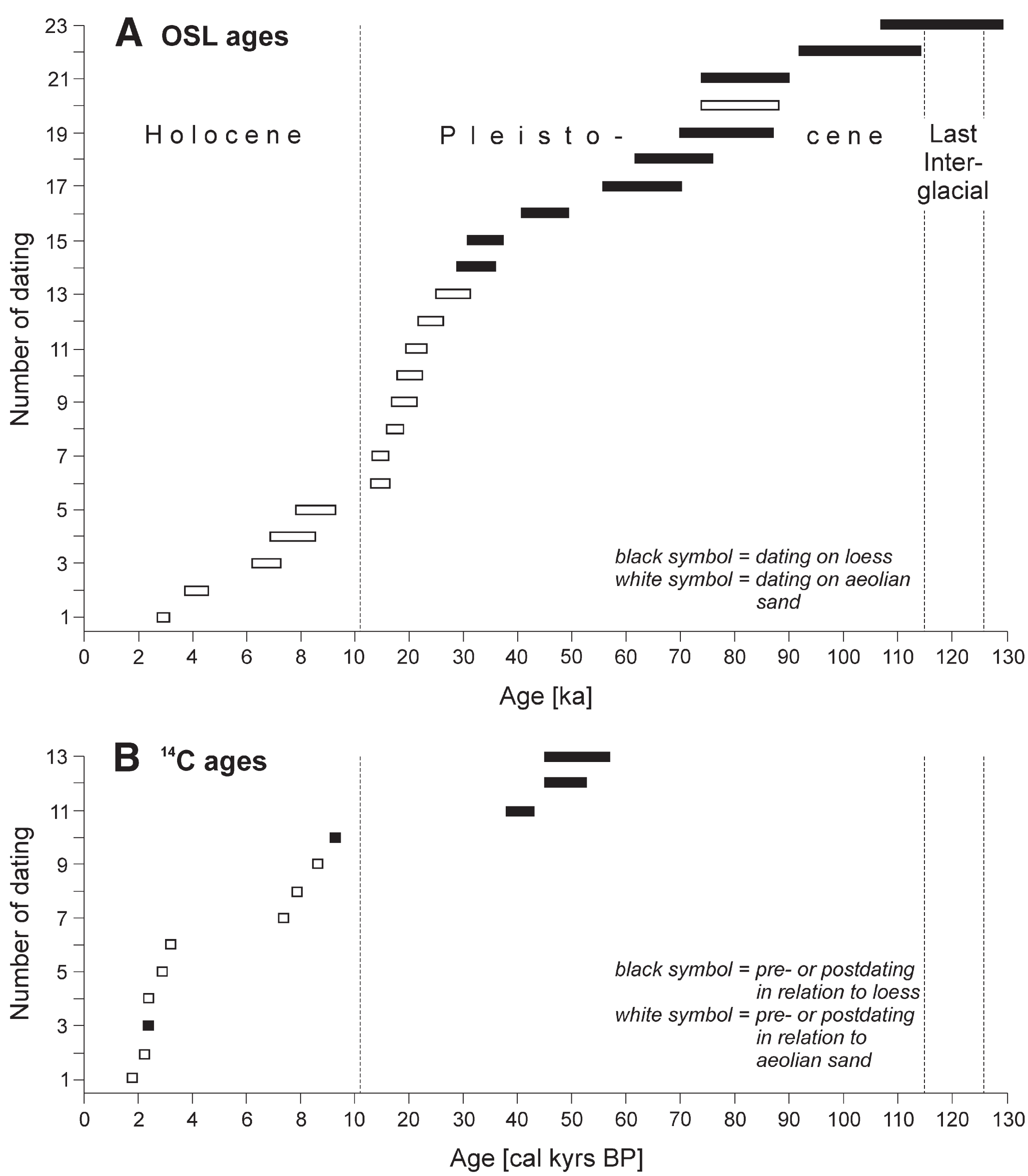

Fig. 6. Dating of aeolian sediments (OSL ages, A) and corresponding palaeosols (^{14}C ages, B) in the Lhasa area. Note the different scaling of the age axis before and after 10 ka / cal kyrs BP.

than the Last Glacial Maximum (LGM, c. 20 ka) and aeolian sands date around the LGM and in the Holocene. However, two ^{14}C ages on palaeosols developed from loess (profiles SAI 1, DRE 9) also point to (secondary?) Holocene loess sedimentation.

Thirteen ^{14}C ages predominately on palaeosols developed from aeolian sand were determined. Most of them date from the Holocene, forming an older cluster (Early to Mid-Holocene) and a younger cluster (Late Holocene; Fig. 6B). In profiles MOG 1 and MOG 4, ^{14}C dates on charcoal from the palaeosols in the lower part of the section yielded ages of 40,305±2312 and 51,024±6148 cal yrs BP respectively. At first glance this suggests that the soils might have been formed during Marine Isotopic Stage (MIS) 3. However, the corresponding OSL ages of >79 ka indicate that these palaeosols were probably formed during the Last Interglacial. Considering the OSL ages available, and keeping in mind the limits of the radiocarbon dating technique (e.g. Geyh, 2005), these ^{14}C age estimates should be regarded as minimum ages only; they may have been contaminated with younger carbon and are at the upper age limit of the technique.

The ^{14}C ages of all other profiles, except QUX 2, seem to be reliable, taking into account the OSL data, the stratigraphical order of the data per profile and the sedimentological properties. Even the ^{14}C age of 48,681±3786 cal yrs BP on charcoal of a palaeosol in profile GYA 3 may be regarded as reliable considering the OSL ages above (44.8±4.0 ka) and below (63.0±7.0 ka). However, in QUX 2 the ^{14}C age of 7784±70 cal yrs BP on charcoal amongst distinctly older OSL ages (16.3±2.0 and 17.2±1.4 ka) is most probably due to a charred root coming from the surface. The youngest sandy-aeolian event detected postdates 1803±61 cal yrs BP (BRI 1; Fig. 3).

5. Discussion

5.1. Past aeolian dynamics and environmental changes

Our dating results reveal an age span of loess deposition from the Last Interglacial (or older) to the Holocene. However, most of the datings fall into the Last Glacial before 34.1±3.0 ka. This finding contradicts the generalised conclusion of Sun et al. (2007), who stated, after OSL dating of four loess sections in the adjacent Yarlung Zhangbo Valley (c. 200 km WSW of Lhasa, with loess basal ages of 11–13 ka) and reviewing previous dating results from a wider area on the Tibetan Plateau, that the present loess in (southern) Tibet had accumulated since the last deglaciation and after the LGM, respectively, suggesting a lack of full-glacial loess. The total number of luminescence ages they used from the whole Plateau amounts to 17.

Actually, there exists a considerably larger dataset of luminescence data on loesses from the Tibetan Plateau (Kaiser, 2007) that point to a different conclusion. As several luminescence studies in north-eastern, eastern and southern Tibet have shown, in fact there is an overwhelming portion of Lateglacial and Holocene loesses (e.g. Lehmkuhl et al., 2000, 2002; Klinge and Lehmkuhl, 2003; Stokes et al., 2003; Klinge and Lehmkuhl, 2005; Küster et al., 2006; Porter and Zhou, 2006). However, more than 50 dates older than c. 15.5 ka (= Lateglacial–Pleniglacial transition) are available predominately ranging between 30 and 80 ka (e.g. Porter et al., 2001; Zhou et al., 2002; Fang et al., 2003; Lu et al., 2004; Madsen et al., 2008). The obvious portion of younger loesses is paralleled by the temporal distribution of ^{14}C-dated palaeosols developed on loess (and mostly overlain by loess as well), which shows a larger quantity of Holocene ages (e.g. Lehmkuhl et al., 2000, 2002; Klinge and Lehmkuhl, 2003, 2005; Porter and Zhou, 2006). Despite a certain amount of unreliable ^{14}C ages on palaeosols coming, for instance, from contamination and re-deposition (e.g. Scharpenseel and Becker-Heidmann, 1992; Martin and Johnson, 1995; Alon et al., 2002), the dominance of (Late) Holocene palaeosol ages appears not in a doubt (Kaiser, 2007).

With respect to the provenance of aeolian dust in the Lhasa area, the relatively coarse-grained loesses with a coarse silt maximum suggest a source that is not distant and certainly rules out a significant component of long-range transported dust. In contrast, loesses on the Chinese Loess Plateau, which are attributed to distant dust sources, show a distinctly finer composition (higher portion of fine and medium silt; Sun et al., 2007). The Th/U ratios of our loess samples except sample DRE 18B show an enrichment of Th in comparison to U ranging from 5.3 to 8.4 (Table 3). A well mixed sedimentary rock of widespread and evolved sources generally shows Th/U ratios of ~3.8 (Taylor and McLennan, 1985). Loess from the Chinese Loess Plateau also shows this characteristic (e.g. Taylor et al., 1983; Jahn et al., 2001), suggesting that this loess represents the average upper continental crust composition. The Loess Plateau sources have been recycled many times and have a wide range of different source rocks as contributors. This implies distant sources rather than proximal ones. In contrast, our loess samples have high Th/U ratios supporting the assumption that the loess sources in the Lhasa area are highly localised, as more distant sources would lead to lower Th/U values. Furthermore, even geochemical and mineralogical data from the adjacent middle reach of the Yarlung Zhangbo Valley indicate a local provenance of loess, essentially resulting from aeolian sorting of fluvial (and glaciofluvial?) deposits. Wind sorting on the braided, sand and silt rich river channels resulted in loess accumulation on the footslopes of the valley flanks (Sun et al., 2007).

In the Lhasa area, the luminescence ages on aeolian sand fall into three groups, probably forming clusters in the Late Pleistocene (around LGM), Early to Mid-Holocene and Late Holocene (Fig. 6A). Even the ^{14}C-dated palaeosols developed from aeolian sand form conspicuous clusters of Early to Mid-Holocene and Late Holocene ages (Fig. 6B). These ^{14}C ages were dominantly obtained from charcoal (absent in underlying strata), which generally indicates burning down of the vegetation and predates sandy-aeolian and colluvial events.

In the introductory chapter, the general question was raised as to whether the Lhasa area could have been influenced by past human activity to the point where it becomes a possible reason for the present treeless desertic environment (vs. a climatic interpretation). The human impact may consist of forest clearing, soil erosion and land degradation (e.g. following cultivation), construction of field terraces and settlements, irrigation, and grazing. In general, the significant increase in fire frequency accompanying human activities is a known phenomenon and is often traced in palaeoenvironmental studies (e.g. Carcaillet and Brun, 2000; Huang et al., 2006). Unfortunately, the usual evidence of environmental change is rarely unambiguous: Charcoal can also come from lightning ignition. However, in the Tibetan ecosystems, which are not characterised by the prevalence of pyrophytes, the human factor is a more likely explanation for the increasing amount of Late Holocene charcoal ages (Miehe et al., 2006; Kaiser, 2007; Miehe et al., 2008a).

In the Kyichu Valley and its tributaries, there is a growing number of known archaeological sites showing the presence of humans since the Late Neolithic (c. 4200 cal yrs BP; Aldenderfer and Zhang, 2004; Kaiser et al., 2006). A much older end Palaeolithic occupation of that area dating into the LGM is discussed in Zhang and Li (2002). As sedentary life since the Neolithic necessarily requires the repeated use of wood and soils and unavoidably triggers local soil erosion by slope runoff and wind, a past human impact on the ecosystem is assumed. Our charcoal findings in the Holocene palaeosols regularly reveal tree species (e.g. juniper, birch), whereas the present-day vegetation mainly consists of sparse grasslands with a few shrubs. The proportion of barren soil, scree and exposed rock is high. However, a few remains of the south-exposed (juniper) and north-exposed (birch, willow) natural forest vegetation still exist (Miehe et al., 2003; Bräuning, 2007; Miehe et al., 2008a), which reveal a present-day 'forest-climate' in that area. The trees are fruiting conspicuously and regeneration is observed where grazing is excluded. In general, the highest present-day treelines in southern and south-western Tibet consisting of juniper are located at 4750 to 4930 m a.s.l. on southeast- and west-exposed slopes (Miehe et al., 2007). The westernmost *Juniperus tibetica* tree was recently found c. 650 km west of the actual forest border at 4850 m a.s.l. (c. 450 km WNW of Lhasa), suggesting that vast areas of now treeless southern Tibet were once forested (Miehe et al., 2006, 2007, 2008a,b). From this it follows that, despite an undoubtedly regional climatic trend of aridification and cooling in the Late Holocene (e.g. Lehmkuhl and Haselein, 2000; Tang et al., 2000; An et al., 2006; Herzschuh, 2006), the Lhasa area is still suitable for bearing forests. Thus the conclusion can be drawn that it is far more difficult to explain the absence of forests by solely climatic causes than accept the hypothesis that humans have destroyed forests and changed this environment to the present desertic pastures over the past millennia. Similar conclusions on a distinct human activity in the Late Holocene have been reported from north-eastern, central and southern Tibet on the basis of analysing aeolian sands (Jäkel, 2002), loesses and palaeosols (Klinge and Lehmkuhl, 2003, 2005), colluvial sediments and palaeosols (Kaiser et al., 2007), surface soils (Kaiser et al., 2008), pollen diagrams (e.g. Frenzel, 2002; Miehe et al., 2006; Schlütz et al., 2007) and present-day vegetation (Miehe et al., 2008a,b,c). However, for the Lhasa area, the question remains open as to whether the *charcoal* ages older than c. 35,000 cal yrs BP (Kaiser et al., in press, this study) can also be attributed to an early activity of humans.

So far, in the catchment of the Kyichu, long-term palaeobotany and palaeoclimatology records covering parts of the Late Quaternary are available only from the so-called 'Hidden Lake' / Co Qongjiamong (c. 140 km ENE of Lhasa, 4980 m a.s.l.; Tang et al., 2000; Shen, 2003), from Damxung (c. 100 km N of Lhasa, 4250 m a.s.l.; Schlütz et al., 2007; Kaiser et al., 2008) and from a peat bog in Lhasa (3650 m a.s.l.; Miehe et al., 2006; Fig. 1). However, new pollen diagrams from that area will be published shortly (La Duo, 2008). The pollen diagrams from 'Hidden Lake' / Co Qongjiamong and Damxung record the last c. 14,000 and 10,500 yrs BP respectively, whereas the Lhasa diagram comprises the last c. 4000 yrs BP only. All diagrams reflect the Holocene presence of trees (e.g. juniper), which partly disappear in the Late Holocene presumably either due to climatic (Tang et al., 2000; Shen, 2003) or anthropogenic causes (Miehe et al., 2006; Schlütz et al., 2007). Unfortunately, there is no palaeoecological information from before c. 14,000 yrs BP available from the study area, except some charcoal determinations revealing rather uncharacteristic shrubs (e.g. *Caragana*, *Sophora*, *Hippophae*; Kaiser et al., in press, this study). However, both the non-glacial sedimentary facies of the profiles presented and the existence of Last Interglacial and Last Glacial palaeosols (e.g. Kastanozems and Calcaric Cambisols in MOG 1 and MOG 4, Regosols and Calcaric Cambisols in GYA 3 and partly DRE 18) show that the valley positions at the altitude studied have been free of glaciers since the Last Interglacial. However, some intervals of that time span certainly have had both colder / drier (LGM; Böhner and Lehmkuhl, 2005) and warmer / moister (MIS 3; Shi et al., 2001) climate conditions implying distinct palaeoenvironmental differences (= soil formation during warm / moist phases vs. possible aeolian sedimentation during cold / dry phases). Regarding regional palaeovegetation, sediments of MIS 3 age reveal tree taxa (e.g. *Pinus*, *Picea*, *Abies*), whereas the LGM is widely characterised by absence of trees (e.g. Shi et al., 2001; Herzschuh et al., 2006). Nevertheless, during the LGM forest-refuge areas seem to have existed in the region of the deep east Tibetan river gorges comprising, for instance, the upper reaches of the Salween, Mekong and Yangtze (Frenzel et al., 2003).

With respect to the rate of the sedimentation process, both lower sedimentation rates in long-term deposition (e.g. c. 2.5 m of Last Glacial loess in profile GYA 3 with c. 0.1 mm yr^{-1}) and higher sedimentation rates in short-term deposition (e.g. c. 10 m of aeolian sand from the LGM in profile CHI 1 with c. 0.5 mm yr^{-1}) were recorded, probably pointing to Late Quaternary changes in the prevailing aeolian process and the vegetation coverage.

In sum, loesses and aeolian sands of partly complex stratigraphic composition are widespread in the study area. The ages yielded represent the oldest dates on aeolian sediments from southern and interior Tibet known so far. This reveals *natural* aeolian sedimentation before and around the LGM. Conversely, a distinct portion of the Late Holocene sandy aeolian sediments, in combination with vegetation changes, is attributed to human-induced *semi-natural* aeolian sedimentation (reactivation of older aeolian sands by grazing and agriculture). Furthermore, whether there was local sandy aeolian sedimentation during the Holocene in the vicinity of wide floodplain sections, probably triggered by high deflation rates, requires investigation.

5.2. Present-day aeolian dynamics and human activity

The Kyichu River transports large amounts of fine and coarse grained sediments comprising an annual sediment discharge of 98,300 t yr^{-1} (Liu and Zhao, 2001). After the summer floods, the floodplains of the Kyichu and its tributaries largely fall dry for the rest of the year. This forms the precondition for subsequent aeolian transport in the valley, triggered by wind channelling effects of the prevailing geomorphology (Fig. 2A). The lower Kyichu Valley in particular, notably its mouth area adjoining the Yarlung Zhangbo, is seasonally influenced by this process. Both field observations of the grain sizes transported and sediments deposited nearby reveal a mainly sandy aeolian transport. There is no present-day loess deposition (and transport) in the Kyichu Valley observable, even on the higher parts of the valley flanks. Thus in the Holocene, neither intensive dust production in close-by sources nor dust input from distant sources can be assumed for the study area.

In contrast, larger areas of active aeolian sands exist, beginning in the southern margins of Lhasa. In contrast to the Yarlung Zhangbo Valley, where vast active dune and coversand fields climb to maximum elevations of nearly 2000 m above the present floodplain (Li et al., 1997; Liu and Zhao, 2001; Sun et al., 2007), areas in the Kyichu Valley consisting of aeolian sand are far less extensive.

According to Liu and Zhao (2001), the area of active aeolian ('shifting') sands in the territory of the middle Yarlung Zhangbo reach and the adjoining Kyichu and Nianchu Valleys (total area = 65,700 km^2) amounts to 578 km^2. This area is distributed over river islands (139 km^2 = 24%), side banks (125 km^2 = 22%), alluvial plains and fans (191 km^2 = 33%), and mountain slopes (123 km^2 = 21%). There is an obvious expanding trend of shifting sandy land in that area with shifting sand dune velocity of 8 to 25 m yr^{-1}. Liu and Zhao (2001) estimated that about 40 km^2 of even the fixed and semi-fixed dunes might be reactivated. They suggested that, besides a natural disposition of that landscape towards sandy aeolian activity, human activities mainly consisting of overgrazing by domestic animals and firewood gathering (esp. *Sophora moorcroftiana*) were chief causes for a present accelerated desertification process. It is estimated that 40–60 km^2 of (semi-) natural vegetation is being cut for fuel every year (Shen and Yang, 1999).

Remarkably, the larger active aeolian sands in the mouth area of the Kyichu are separated from the floodplain by a strip of varying width of irrigated arable land and woodlands also containing several villages (Appendix A). As shown by the lack of traces of aeolian sand transported laterally *through* this strip, it obviously forms an effective barrier to aeolian sand transport from the floodplain to the slopes. On the one hand, the ages of aeolian sands in profiles CHI 1 and JIN 2, which lie in *active* aeolian sand areas, widely reveal a Pleistocene age of aeolian deposition. Obviously, human activity in the form of the above-mentioned processes can be claimed for a modern *reactivation* of the uppermost portion of old deposits. On the other hand, both the OSL ages and the ^{14}C pre- / postdatings on palaeosols yielding Holocene ages (e.g. STA 1, BRI 1, DAR 1) reveal local sandy aeolian activity for the very Late Holocene again possibly caused by human activity.

In summary, both the conclusions on the aeolian dynamics (widespread Pleistocene loess and aeolian sand deposition, local Late Holocene aeolian sand deposition, recent reactivation of widespread Pleistocene aeolian sands) and the palaeobotanical results (vegetation change from a tree-bearing to a widely treeless landscape) provide evidence that the Lhasa area was already strongly influenced by human activity at the beginning of the Late Holocene. Thus, the present-day desertic environment at the altitude investigated (c. 3540–4580 m a.s.l.) does not result primarily from the semiarid climate or the high-altitude conditions but from activities of the humans and their collateral effects. However, once established, this semi-natural ecosystem persists, controlled by strong grazing, fire-wood extraction, erosion and harsh edaphic conditions for the recovery of tree species. Accordingly, and proven by first experimental results (Liu and Zhao, 2001; Miehe et al., 2003), a complex set of measures, such as exclusion of grazing animals, cessation of wood-cutting and afforestation with site-adapted trees, is required to restore the potentially natural ecosystems: broadly speaking, mixed woodlands.

6. Conclusions

(1) At the altitude studied (3540–4580 m a.s.l.), nearly the whole landscape is covered by a mostly thin veneer (<1 m) of aeolian sediments. Only locally, particularly on footslope positions and in aeolian sand areas, does the thickness of loesses and aeolian sands exceed 5 m, reaching a maximal thickness of more than 9 m and 12 m respectively. The spatially predominant aeolian sediment is loess.

(2) The majority of the loess layers investigated have a massive structure without visible layering, thus widely excluding a major component of reworking. They partly contain carbonate and exclusively represent the 'silt loam' textural class, having the prevalent percentage in the coarse silt fraction. The mostly carbonate-free aeolian sands represent a wide range of textural classes (sands, loams), having the dominant fraction in the fine sand category. Sediment properties of both loesses and aeolian sands reveal an origin from aeolian sorting of nearby fluvial deposits. Buried palaeosols of different types developed from aeolian sediments regularly occur, representing temperate to cool and humid to semiarid site conditions during pedogenesis. Analytical parameters of aeolian sediments, palaeosols and surface soils indicate non-saline site conditions.

(3) OSL dating reveals an age span of loess deposition from the Last Interglacial to the Early Holocene, but most of the ages fall into the Last Glacial, *before* the LGM. This finding contradicts previous conclusions that loess in southern Tibet had accumulated exclusively *after* the LGM. At present, there is no loess sedimentation in the study area. OSL datings on aeolian sand fall into three groups clustering in the Late Pleistocene (around LGM), Early to Mid-Holocene and Late Holocene. ^{14}C age estimates of palaeosols developed from aeolian sand cluster in the Early to Mid-Holocene and in the Late Holocene. Recently, larger areas of active sandy aeolian dynamics occur in the mouth area of the Kyichu River adjoining the Yarlung Zhangbo Valley, which are interpreted to be caused by human-induced reactivation of mainly Late Pleistocene aeolian sands.

(4) The charcoal spectra analysed give evidence of a Late Holocene change from a tree- and shrub-dominated vegetation to the present plant cover, consisting of sparse grasses, herbs and dwarf shrubs. This vegetation change in combination with proven agricultural activity since the Late Neolithic (c. 4200 cal yrs BP) suggests that the Lhasa area was already strongly influenced by human activity at the beginning of the Late Holocene. Thus, the present-day desertic environment might not result primarily from the semiarid climate or the high-altitude conditions, but from the past and present-day activities of humans and their collateral effects.

Acknowledgements

We are indebted to Werner H. Schoch, Langnau, for the botanical charcoal determination. Stefan Reiss, Marburg, assisted in carrying out soil analyses. We also thank Christiane Enderle, Marburg, for the preparation of Fig. 1, and James Fanning, Greifswald, for improving the English. We owe two anonymous reviewers constructive reviews, which improved the quality of the paper. Research as well as print of the colour figures was kindly supported by the German Research Foundation (DFG KA 2713/1-1). Zhongping Lai is indebted to the German Alexander von Humboldt Foundation for a fellowship allowing OSL research in the Marburg Luminescence Laboratory.

Appendix A. Supplementary data

Supplementary data associated with this article can be found, in the online version, at doi:10.1016/j.palaeo.2008.11.004.

References

Aldenderfer, M., Zhang, Y.N., 2004. The prehistory of the Tibetan Plateau to the seventh century A.D.: perspectives and research from China and the West since 1950. Journal of World Prehistory 18, 1–55.

Alon, D., Mintz, G., Cohen, I., Weiner, S., Boaretto, E., 2002. The use of Raman spectroscopy to monitor the removal of humic substances from charcoal: quality control for ^{14}C dating of charcoal. Radiocarbon 44, 1–11.

An, Z.S., Kukla, G.J., Porter, S.C., Xiao, J.L., 1991. Late Quaternary dust flow on the Chinese Loess Plateau. Catena 18, 125–132.

An, C.B., Feng, Z.D., Barton, L., 2006. Dry or humid? Mid-Holocene humidity changes in arid and semi-arid China. Quaternary Science Reviews 25, 351–361.

Atlas of Tibet Plateau, 1990. Edited by the Institute of Geography, Chinese Academy of Sciences. Beijing (in Chinese).

Böhner, J., Lehmkuhl, F., 2005. Environmental change modelling for Central and High Asia: Pleistocene, present and future scenarios. Boreas 34, 220–231.

Bräuning, A., 2007. Dendroecological studies on the Tibetan Plateau. Implications of relict juniper forests for climate change and cultural history. Geographische Rundschau International Edition 3, 38–43.

Brown, L.R., 2003. China's war with the desert. New Perspectives Quarterly 20, 77–78.

Carcaillet, C., Brun, J.-J., 2000. Changes in landscape structure in the northwestern Alps over the last 7000 years: lessons from soil charcoal. Journal of Vegetation Science 11, 705–714.

Clarke, M.L., 1995. Sedimentological characteristics and rare earth element fingerprinting of Tibetan silts and their relationship with the sediments of the western Chinese Loess Plateau. In: Derbyshire, E. (Ed.), Wind Blown Sediments in the Quaternary Record. Quaternary Proceedings, vol. 4, pp. 41–51.

Ding, Z.L., Derbyshire, E., Yang, S.L., Sun, J.M., Liu, T.S., 2005. Stepwise expansion of desert environment across northern China in the past 3.5 Ma and implications for monsoon evolution. Earth and Planetary Science Letters 237, 45–55.

Domrös, M., Peng, G., 1988. The Climate of China. Springer, Berlin.

Fang, X.M., Lü, L.Q., Mason, J.A., Yang, S.L., An, Z.S., Li, J.J., Guo, Z.L., 2003. Pedogenic response to millennial summer monsoon enhancements on the Tibetan Plateau. Quaternary International 106–107, 79–88.

FAO, 2006. Guidelines for Soil Description, 4th edition. FAO, Rome.

Frenzel, B., 2002. History of flora and vegetation during the Quaternary. Progress in Botany 63, 368–385.

Frenzel, B., Bräuning, A., Adamczyk, S., 2003. On the problem of possible last-glacial forest-refuge-areas within the deep valleys of eastern Tibet. Erdkunde 57, 182–198.

Geyh, M., 2005. ^{14}C dating – still a challenge for users? Zeitschrift für Geomorphologie Supplement 139, 63–86.

He, X.B., Zhou, J., Zhang, X.B., Tang, K.L., 2006. Soil erosion response to climatic change and human activity during the Quaternary on the Loess Plateau, China. Regional Environmental Change 6, 62–70.

Herzschuh, U., 2006. Palaeo-moisture evolution in monsoonal Central Asia during the last 50,000 years. Quaternary Science Reviews 25, 163–178.

Herzschuh, U., Kürschner, H., Mischke, S., 2006. Temperature variability and vertical vegetation belt shifts during the last ~50,000 yr in the Qilian Mountains (NE margin of the Tibetan Plateau, China). Quaternary Research 66, 133–146.

Huang, C.C., Pang, J.L., Chen, S., Su, H.X., Han, J.A., Cao, Y.F., Zhao, W.Y., Tan, Z.H., 2006. Charcoal records of fire history in the Holocene loess-soil sequences over the southern Loess Plateau of China. Palaeogeography, Palaeoclimatology, Palaeoecology 239, 28–44.

IUSS-ISRIC-FAO, 2006. World Reference Base for Soil Resources. A Framework for International Classification, Correlation and Communication. World Soil Resources Reports, vol. 103. FAO, Rome.

Jahn, B.M., Gallet, S., Han, J.M., 2001. Geochemistry of the Xining, Xifeng and Jixian sections, Loess Plateau of China: eolian dust provenance and paleosol evolution during the last 140 ka. Chemical Geology 178, 71–94.

Jäkel, D., 2002. Storeys of aeolian relief in North Africa and China. In: Yang, X.P. (Ed.), Desert and Alpine Environments. Advances in Geomorphology and Palaeoclimatology. China Ocean Press, Beijing, pp. 6–21.

Kaiser, K., 2007. Soils and terrestrial sediments as indicators of Holocene environmental changes on the Tibetan Plateau. Habilitation thesis (postdoctoral lecture qualification), Faculty of Geography, University of Marburg (Germany).

Kaiser, K., Miehe, G., Schoch, W.H., Zander, A., Schlütz, F., 2006. Relief, soil and lost forests: Late Holocene environmental changes in southern Tibet under human impact. Zeitschrift für Geomorphologie Supplement 142, 149–173.

Kaiser, K., Schoch, W.H., Miehe, G., 2007. Holocene paleosols and colluvial sediments in Northeast Tibet (Qinghai Province, China): properties, dating and paleoenvironmental implications. Catena 69, 91–102.

Kaiser, K., Miehe, G., Barthelmes, A., Ehrmann, O., Scharf, A., Schult, M., Schlütz, F., Adamczyk, S., Frenzel, B., 2008. Turf-bearing topsoils on the central Tibetan Plateau, China: pedology, botany, geochronology. Catena 73, 300–311.

Kaiser, K., Lai, Z.P., Schneider, B., Schoch, W.H., Shen, X.H., Miehe, G., Brückner, H., in press. Sediment sequences and paleosols in the Kyichu Valley, southern Tibet (China), indicating Late Quaternary environmental changes. Island Arc doi:10.1111/j.1440-1738.2008.00629.x.

Kemp, R.A., Derbyshire, E., Chen, F.H., Ma, H.Z., 1996. Pedosedimentary development and palaeoenvironmental significance of the S1 palaeosol on the northeastern margin of the Qinghai–Xizang (Tibetan) Plateau. Journal of Quaternary Science 11, 95–106.

Klinge, M., Lehmkuhl, F., 2003. Paleosols and aeolian mantles in southern and eastern Tibet – Results and implications for Late Quaternary climatic change. Berliner Paläobiologische Abhandlungen 2, 62–64.

Klinge, M., Lehmkuhl, F., 2005. Untersuchungen zur holozänen Bodenentwicklung und Geomorphodynamik in Tibet – Hinweise auf klimatische und anthropogene Veränderungen. Berliner Geographische Arbeiten 100, 81–91.

Krasilnikov, P., Garcia Calderon, N.E., 2006. A WRB-based buried paleosol classification. Quaternary International 156–157, 176–188.

Küster, Y., Hetzel, R., Krbetschek, M., Tao, M.X., 2006. Holocene loess sedimentation along the Qilian Shan (China): significance for understanding the processes and timing of loess deposition. Quaternary Science Reviews 25, 114–125.

La Duo, 2008. Studies in the ecology and palaeoecology of the Lhasa Valley, Tibet Autonomous Region, China. Ph.D. thesis, Department of Biology, University of Bergen (Norway).

Lai, Z.P., Wintle, A.G., 2006. Locating the boundary between the Pleistocene and the Holocene in Chinese loess using luminescence. The Holocene 16, 893–899.

Lai, Z.P., Brückner, H., 2008. Effects of feldspar contamination on equivalent dose and the shape of growth curve for OSL of silt-sized quartz extracted from Chinese loess. Geochronometria 30, 49–53.

Lai, Z.P., Wintle, A.G., Thomas, D.S.G., 2007. Rates of dust deposition between 50 ka and 20 ka revealed by OSL dating at Yuanbao on the Chinese Loess Plateau. Palaeogeography, Palaeoclimatology, Palaeoecology 248, 431–439.

Lai, Z.P., Zöller, L., Fuchs, M., Brückner, H., 2008. Alpha efficiency determination for OSL of quartz extracted from Chinese loess. Radiation Measurements 43, 767–770.

Lehmkuhl, F., 1995. Geomorphologische Untersuchungen zum Klima des Holozäns und Jungpleistozäns Osttibets. Göttinger Geographische Abhandlungen 102.

Lehmkuhl, F., 1997. The spatial distribution of loess and loess-like sediments in the mountain areas of Central and High Asia. Zeitschrift für Geomorphologie Supplement 111, 97–116.

Lehmkuhl, F., Haselein, F., 2000. Quaternary palaeoenvironmental change on the Tibetan Plateau and adjacent areas (Western China and Western Mongolia). Quaternary International 65–66, 121–145.

Lehmkuhl, F., Klinge, M., Rees-Jones, J., Rhodes, E.J., 2000. First luminescence dates for Late Quaternary aeolian sedimentation in Central and Eastern Tibet. Quaternary International 68–71, 121–141.

Lehmkuhl, F., Klinge, M., Lang, A., 2002. Late Quaternary glacier advances, lake level fluctuations and aeolian sedimentation in Southern Tibet. Zeitschrift für Geomorphologie Supplement 126, 183–218.

Li, S., Wang, Y., Ha, S., Yang, P., Jin, H.L., Zhang, J.S., 1997. Classification and development of aeolian sand landform in the Yurlung Zangbo valley. Journal of Desert Research 17, 342–350 (in Chinese).

Li, F.R., Kang, L.F., Zhang, H., Zhao, L.Y., Shirato, Y., Taniyama, I., 2005. Changes in intensity of wind erosion at different stages of degradation development in grasslands of Inner Mongolia, China. Journal of Arid Environments 62, 567–585.

Li, X.O., Yi, C.L., Chen, F.H., Yao, T.D., Li, X., 2006. Formation of proglacial dunes in front of the Puruogangri Icefield in the central Qinghai–Tibet Plateau: Implications for reconstructing paleoenvironmental changes since the Lateglacial. Quaternary International 154–155, 122–127.

Liu, Z.M., Zhao, W.Z., 2001. Shifting sand control in Central Tibet. Ambio 30, 376–380.

Lu, H.Y., Wang, X.Y., Ma, H.Z., Tan, H.B., Vandenberghe, J., Miao, X.D., Li, Z., Sun, Y.B., An, Z.S., Cao, G.C., 2004. The Plateau Monsoon variation during the past 130 kyr revealed by loess deposit at north-east Qinghai–Tibet (China). Global and Planetary Change 41, 207–214.

Luo, T.X., Brown, S., Pan, Y.D., Shi, P.L., Hua, O.Y., Yu, Z.L., Zhu, H.Z., 2005. Root biomass along sub-tropical to alpine gradients: global implication from Tibetan transect studies. Forest Ecology and Management 206, 349–363.

Madsen, D.B., Ma, H.Z., Rhode, D., Brantingham, P.J., Forman, S.L., 2008. Age constraints on the late Quaternary evolution of Qinghai Lake, Tibetan Plateau. Quaternary Research 69, 316–325.

Martin, C.W., Johnson, W.C., 1995. Variation in radiocarbon ages of soil organic matter fractions from Late Quaternary buried soils. Quaternary Research 43, 232–237.

Miehe, G., Winiger, M., Böhner, J., Zhang, Y.L., 2001. The climatic diagram map of High Asia. Purpose and concepts. Erdkunde 55, 94–97.

Miehe, G., Miehe, S., Koch, K., Will, M., 2003. Sacred Forests in Tibet. Using geographical information systems for forest rehabilitation. Mountain Research and Development 23, 324–328.

Miehe, G., Miehe, S., Schlütz, F., Kaiser, K., La Duo, 2006. Palaeoecological and experimental evidence of former forests and woodlands in the treeless desert pastures of Southern Tibet (Lhasa, A.R. Xizang, China). Palaeogeography, Palaeoclimatology, Palaeoecology 242, 54–67.

Miehe, G., Miehe, S., Vogel, J., Sonam Co, La Duo, 2007. Highest treeline in the northern hemisphere found in southern Tibet. Mountain Research and Development 27, 169–173.

Miehe, G., Miehe, S., Will, M., Opgenoorth, L., La Duo, Tsering Dorgeh, Liu, J.Q., 2008a. An inventory of forest relics in the pastures of Southern Tibet (Xizang A.R., China). Plant Ecology 194, 157–177.

Miehe, G., Miehe, S., Kaiser, K., Liu, J.Q., Zhao, X.Q., 2008b. Status and dynamics of the *Kobresia pygmaea* ecosystem on the Tibetan Plateau. Ambio 37, 272–279.

Miehe, G., Kaiser, K., Sonam Co, Zhao, X.Q., Liu, J.Q., 2008c. Geo-ecological transect studies in northeast Tibet (Qinghai, China) reveal human-made mid-Holocene environmental changes in the upper Yellow River catchment changing forest to grassland. Erdkunde 62, 187–199.

Murray, A.S., Wintle, A.G., 2000. Luminescence dating of quartz using an improved single-aliquot regenerative-dose protocol. Radiation Measurements 32, 57–73.

Nettleton, W.D., Olson, C.G., Wysocki, D.A., 2000. Paleosol classification: problems and solutions. Catena 41, 61–92.

Pessenda, L.C.R., Gouveia, S.E.M., Aravena, R., 2001. Radiocarbon dating of total soil organic matter and humin fraction and its comparison with ^{14}C ages of fossil charcoal. Radiocarbon 43, 595–601.

Péwé, T.L., Liu, T.S., Slatt, R.M., Li, B.Y., 1995. Origin and character of loesslike silt in the southern Qinghai–Xizang (Tibet) Plateau, China. US Geological Survey Professional Paper 1549.

Porter, S.C., Zhou, W.J., 2006. Synchronism of Holocene East Asian monsoon variations and North Atlantic drift-ice tracers. Quaternary Research 65, 443–449.

Porter, S.C., Singhvi, A., An, Z.S., Lai, Z.P., 2001. Luminescence age and palaeoenvironmental implications of a Late Pleistocene ground wedge on the Northeastern Tibetan Plateau. Permafrost and Periglacial Processes 12, 203–210.

Prescott, J.R., Hutton, J.T., 1994. Cosmic ray contributions to dose rates for luminescence and ESR dating: large depths and long-term time variations. Radiation Measurements 23, 497–500.

Pye, K., 1995. The nature, origin and accumulation of loess. Quaternary Science Reviews 14, 653–667.

Scharf, A., Uhl, T., Luppold, W., Rottenbach, A., Kritzler, K., Ohneiser, A., Kretschmer, W., 2007. Status report on the Erlangen AMS facility. Nuclear Instruments and Methods in Physics Research B 259, 50–56.

Scharpenseel, H.W., Becker-Heidmann, P., 1992. Twenty five years of radiocarbon dating soils: paradigm of erring and learning. Radiocarbon 34, 541–549.

Schlütz, F., Miehe, G., Lehmkuhl, F., 2007. Zur Geschichte des größten alpinen Ökosystems der Erde – Palynologische Untersuchungen zu den *Kobresia*-Matten SE-Tibets. Berichte der Reinhold-Tüxen-Gesellschaft 19, 17–30.

Shen, C.M., 2003. Millennial-scale variations and centennial-scale events in the southwest Asian monsoon: pollen evidence from Tibet. PhD thesis, Louisiana State University, Baton Rouge (USA).

Shen, W.S., Yang, P., 1999. Land desertification and its developing trends in the Lhasa area, Tibet. Journal of Desert Research 19, 33–37 (in Chinese).

Shi, Y.F., Yu, G., Liu, X.D., Li, B.Y., Yao, T.D., 2001. Reconstruction of the 30–40 ka BP enhanced Indian monsoon climate based on geological records from the Tibetan Plateau. Palaeogeography, Palaeoclimatology, Palaeoecology 169, 69–83.

Song, M.H., Zhou, C.P., Hua, O.Y., 2004. Distributions of dominant tree species on the Tibetan Plateau under current and future climate scenarios. Mountain Research and Development 24, 166–173.

Stokes, S., Hetzel, R., Bailey, R.M., Tao, M.X., 2003. Combined IRSL–OSL single aliquot regeneration (SAR) equivalent dose (De) estimates from source proximal Chinese loess. Quaternary Science Reviews 22, 975–983.

Sun, J.M., Li, S.H., Han, P., Chen, Y.Y., 2006. Holocene environmental changes in the central Inner Mongolia, based on single-aliquot-quartz optical dating and multi-proxy study of dune sands. Palaeogeography, Palaeoclimatology, Palaeoecology 233, 51–62.

Sun, J.M., Li, S.H., Muhs, D.R., Li, B., 2007. Loess sedimentation in Tibet: provenance, processes, and link with Quaternary glaciations. Quaternary Science Reviews 26, 2265–2280.

Tang, L.Y., Shen, C.M., Liu, K.B., Overpeck, J.T., 2000. Changes in South Asian monsoon: new high-resolution paleoclimatic records from Tibet, China. Chinese Science Bulletin 45, 87–90.

Taylor, S.R., McLennan, S.M., 1985. The Continental Crust: Its Composition and Evolution. Blackwell Scientific Publications, Oxford.

Taylor, S.R., McLennan, S.M., McCulloch, M.T., 1983. Geochemistry of loess, continental crustal composition and crustal model ages. Geochimica et Cosmochimica Acta 47, 1897–1905.

Weninger, B., Jöris, O., Danzeglocke, U., 2007. CalPal-2007. Cologne Radiocarbon Calibration & Palaeoclimate Research Package. http://www.calpal.de.

Yang, X.P., Rost, K.T., Lehmkuhl, F., Zhenda, Z., Dodson, J., 2004. The evolution of dry lands in northern China and in the Republic of Mongolia since the Last Glacial Maximum. Quaternary International 118–119, 69–85.

Yu, G., Tang, L.Y., Yang, X.D., Ke, X.K., Harrison, S.P., 2001. Modern pollen samples from alpine vegetation on the Tibetan Plateau. Global Ecology and Biogeography 10, 503–519.

Zhang, D.D., Li, S.H., 2002. Optical dating of Tibetan human hand- and footprints: an implication for the palaeoenvironment of the last glaciation of the Tibetan Plateau. Geophysical Research Letters 29, 1072–1074.

Zhou, S.Z., Li, J.J., Zhang, S.Q., 2002. Quaternary glaciation of the Bailang River Valley, Qilian Shan. Quaternary International 97–98, 103–110.